Received: 13 February 2018 | Revised: 16 June 2018 | Accepted: 19 June 2018

DOI: 10.1002/stc.2234

RESEARCH ARTICLE

WILEY

Improving the dynamic performance of base-isolated structures via tuned mass damper and inerter devices: A comparative study

Dario De Domenico | Giuseppe Ricciardi

Department of Engineering, University of Messina, Messina, Italy

Correspondence
Dario De Domenico, Department of Engineering, University of Messina, Contrada Di Dio, 98166 Sant'Agata, Messina, Italy.
Email: dario.dedomenico@unime.it

Funding information
Italian Ministry of Education, University and Research, Grant/Award Numbers: 2015JW9NJT and 2015TTJN95

Summary

The dynamic performance of base-isolated buildings can be improved by introducing a tuned mass damper (TMD) at basement, below the isolation floor where most of the earthquake-induced displacement demand is concentrated. In order to enhance the effectiveness of the TMD without simultaneously amplifying the relevant mass ratio, the use of supplemental inertial mass dampers has been envisaged by the authors and other authors in earlier studies. These schemes exploit the mass-amplification effect of the inerter, a two-terminal device whose generated force is ideally proportional to the relative acceleration between its terminals. In this paper, we present a review along with a systematic comparative study of six different strategies proposed in the literature, each one featuring a specific combination of mass-spring-dashpot elements arranged in series or in parallel with an inerter for the displacement mitigation of base-isolated structures. Frequency-response functions of each model are derived in closed form. Optimal design is based on a common strategy, considering a white-noise random process as seismic input, by minimization of the displacement variance but with an eye also for the superstructure acceleration (associated with forces arising in the superstructure) and for the TMD stroke. Then, the seismic performance of the six systems is assessed considering an ensemble of 52 natural earthquake ground motions, by comparing several response indicators including TMD stroke, deformation of the base-isolation floor, superstructure acceleration, interstory drifts, base shear, and reactions associated with spring, oil damper, and inertial damper supporting the TMD, which are significant for outlining preliminary economic assessments.

KEYWORDS

base isolation, earthquake protection, hybrid structural control, inerter, optimal design, tuned mass damper

1 | INTRODUCTION

Seismic base isolation has proven to be an effective earthquake protection strategy for building structures.[1,2] However, there has been a growing interest towards so-called *hybrid* control strategies combining the conventional base-isolation

system (BIS) with other active or passive control systems. Indeed, a few shortcomings may be encountered by the BIS alone, mainly the large displacements concentrated at the isolation floor (which may induce risk of pounding[3]) and the vulnerability to long-period ground motions.[4-6]

To overcome these drawbacks, some *hybrid* control strategies have been proposed in the literature. One of the most popular solutions combines the BIS with a *tuned mass damper* (TMD) that is attached immediately above or below the isolation floor.[7-10] Based on a similar concept, the effect of a tuned liquid column damper installed at the base of a base-isolated structures was also studied recently.[11,12] It is well known that the effectiveness of TMD-like systems is related to the mass employed: For instance, in Casciati and Giuliano,[13] a poor seismic performance of multiple TMDs with small mass ratios was reported with regard to seismic excitation. Although this strategy is effective for wind engineering, see, for example, Casciati and Giuliano[13] and Bortoluzzi et al,[14] the convenience of the TMD in seismic engineering is still controversial.[15]

In order to improve the performance of the TMD, which is related to the TMD mass employed, more recently, the TMD has been studied in conjunction with the *inerter*,[16] also termed inertial mass damper,[17] gyro-mass damper,[18] or simply mass damper[19] in the literature. The inerter resisting force is ideally proportional to the relative acceleration of its two terminals: It acts as an additional, apparent mass for the system it is connected to. By exploiting the concept of rotational inertia[20-22] and the resulting mass-amplification effect of the inerter, lower mass and more effective alternatives to the traditional TMD arise, that is, the tuned mass damper inerter (TMDI)[23-25] and the tuned inerter damper (TID)[26-29]: In the former, the device inertance substitutes the mass of the TMD partly; in the latter, it plays the role of the TMD mass entirely. The TMDI is a more robust and effective system than the TMD, as the mass amplification effect of the inerter reduces the performance sensitivity to the tuning frequency and to the earthquake frequency content.[24] This attractive feature mitigates some of the well-known shortcomings of the TMD for earthquake engineering applications.

The aim of this paper is to present a review and to make a comparison of different hybrid control strategies in this field. Considering the previous remarks and the advantageous properties of the inerter in TMD systems, it seems interesting to overview the hybrid control strategies proposed in the literature so far, in order to assess, within a unified comparative study, the different seismic performance and behavior of alternative dynamic layouts. Indeed, different arrangements of TMD and inerter in conjunction with the BIS give rise to a totally different dynamic behavior. For example, if the inerter is placed in between the TMD and the BIS, it mainly reduces the TMD stroke, whereas if it is connected in between the TMD mass and the ground, it controls the excessive displacement demand of the isolators. Therefore, in order to complete some previous research work,[30,31] we here expand the investigation of TMD-like systems with and without inerter in conjunction with BISs by comprising six alternative structural control layouts having different characteristics.[32-34] As a first novel contribution of this paper, closed-form expressions for the frequency-response functions of each model are derived. Some of the analyzed models were proposed in the literature, but no indications on the optimal tuning were given. As a second novel contribution of this paper, we provide guidelines and design graphs for the selection of the optimal design parameters of each model based on a common, unified strategy. More specifically, the tuning procedure is carried out for all the six models considering a stationary white-noise random process as seismic input, by minimization of the displacement variance but with an eye also for the acceleration variance (associated with forces arising in the superstructure) and for the TMD stroke variance, in order to achieve an overall and effective structural control. The validity of the proposed optimal design strategy is then assessed in the time domain, by considering a wide variety of characteristics of the seismic signal (frequency content, duration, nonstationary nature, etc.), in line with the indications in Giuliano.[15] To this aim, response-history analyses of a base-isolated multistory building are performed under 52 real accelerograms with different spectral characteristics. The performance of the six models is analyzed in terms of a broad group of response indicators, including TMD stroke, deformation of the base-isolation floor, superstructure acceleration, interstory drifts, base shear, and reactions associated with the spring, oil damper, and inertial damper supporting the TMD, which are significant for drawing preliminary assessments in terms of costs and effectiveness of each structural control strategy in a comparative manner.

2 | BASE ISOLATION WITH TMD AND INERTER

Reference is made to the simple sketch shown in Figure 1. The combined system is subject to the horizontal ground acceleration $\ddot{u}_g(t)$. A single-degree-of-freedom (SDOF) system is considered for the superstructure (mass m_s, damping c_s, stiffness k_s, and displacement, relative to the ground, u_s)—this SDOF may be representative of the fundamental mode of vibration of a multi–degree-of-freedom (MDOF) structural system, which is usually referred to for a preliminary

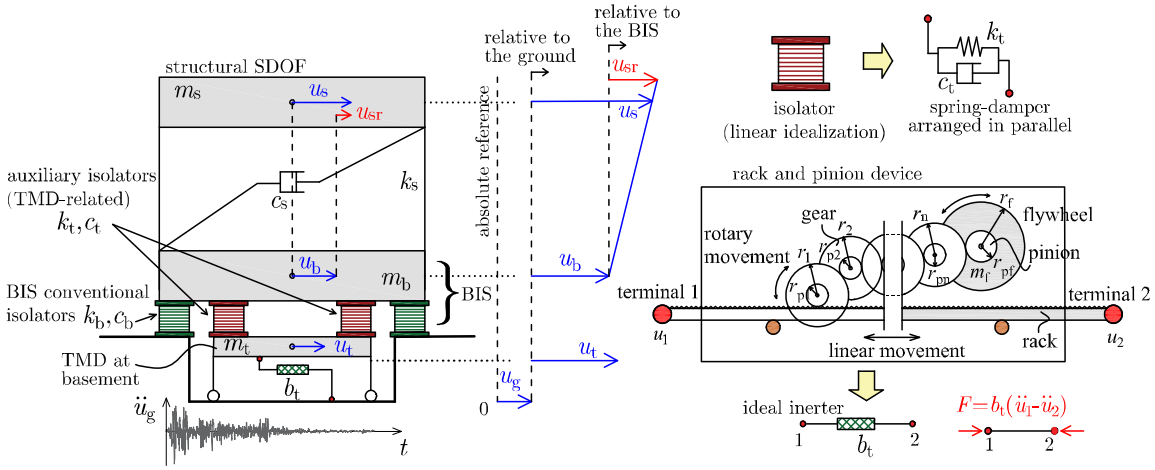

FIGURE 1 Base-isolated single-degree-of-freedom (SDOF) system with attached tuned mass damper (TMD) and inertial damper: Conventions for displacements and schematic models for isolators and inerter. BIS: base-isolation system

design of the TMD parameters in MDOF systems. The BIS is idealized as another SDOF (displacement u_b relative to the ground) interconnected to the structural SDOF and featured by parameters m_b, c_b, k_b.[35] The third DOF, identified by a displacement u_t relative to the ground, pertains to the TMD that is represented by a secondary mass m_t located at basement and attached to the isolation floor via spring k_t and damper c_t. According to the notation adopted in De Domenico and Ricciardi,[30] the spring and damper properties k_t, c_t associated with the TMD can be meant as the effective stiffness and equivalent viscous damping of an *auxiliary* set of isolators in addition to the conventional isolators (featured by k_b, c_b) as sketched in Figure 1. Finally, the inertial damper is represented by a hatched box, whose resisting force is proportional to the relative acceleration between its two terminals

$$F_{\text{inerter}} = b_t(\ddot{u}_1 - \ddot{u}_2), \tag{1}$$

where the constant b_t, having dimension of a mass, is called *inertance*. This device idealization can be practically realized in several ways, for instance, via a combined arrangement of rack, pinions, gears, and flywheel as shown in Figure 1. In this case, the inertance of the system is expressed as

$$b_t = m_f \frac{r_f^2}{r_{pf}^2}\left(\prod_{i=1}^{n}\frac{r_i^2}{r_{pi}^2}\right), \tag{2}$$

where n is the number of gears, m_f is the flywheel mass, and r_i, r_{pi}, r_f, and r_{pf} denote the radius of gears, pinions, flywheel, and flywheel pinion, respectively. Linear movement of the rack generates rotational movement in gears and flywheel, and the rotational inertia can be amplified by adjusting the gearing ratios in Eq. (2), or simply introducing additional gears to attain very high values of the inertance b_t. Such *mass amplification effect* is the key feature of this system and makes it appealing for vibration control purposes.

3 | REVIEW OF BASE-ISOLATED STRUCTURAL CONTROL SYSTEMS WITH TMD AND INERTER

In Figure 2, six different models of base-isolated SDOFs with different arrangements of TMD and inertial dampers are depicted. In an attempt to describe these models in a unified manner for the present comparative study, the equations of motion are all expressed as

$$\mathbf{M}\ddot{\mathbf{u}}(t) + \mathbf{C}\dot{\mathbf{u}}(t) + \mathbf{K}\mathbf{u}(t) = -\boldsymbol{\tau}\ddot{u}_g(t), \tag{3}$$

with $\mathbf{M}$, $\mathbf{C}$, $\mathbf{K}$ being the mass, damping, and stiffness matrix, respectively; $\mathbf{u}(t)^T = [u_{sr}, u_b, u_t]$ the vector collecting the three DOFs of the systems; and $\boldsymbol{\tau}^T = [m_s,\ m_s + m_b,\ m_t]$ the influence vector. Expressing the equations of motion in terms of the relative displacement of the m_s mass with respect to the BIS $u_{sr} = u_s - u_b$, rather than to the displacement

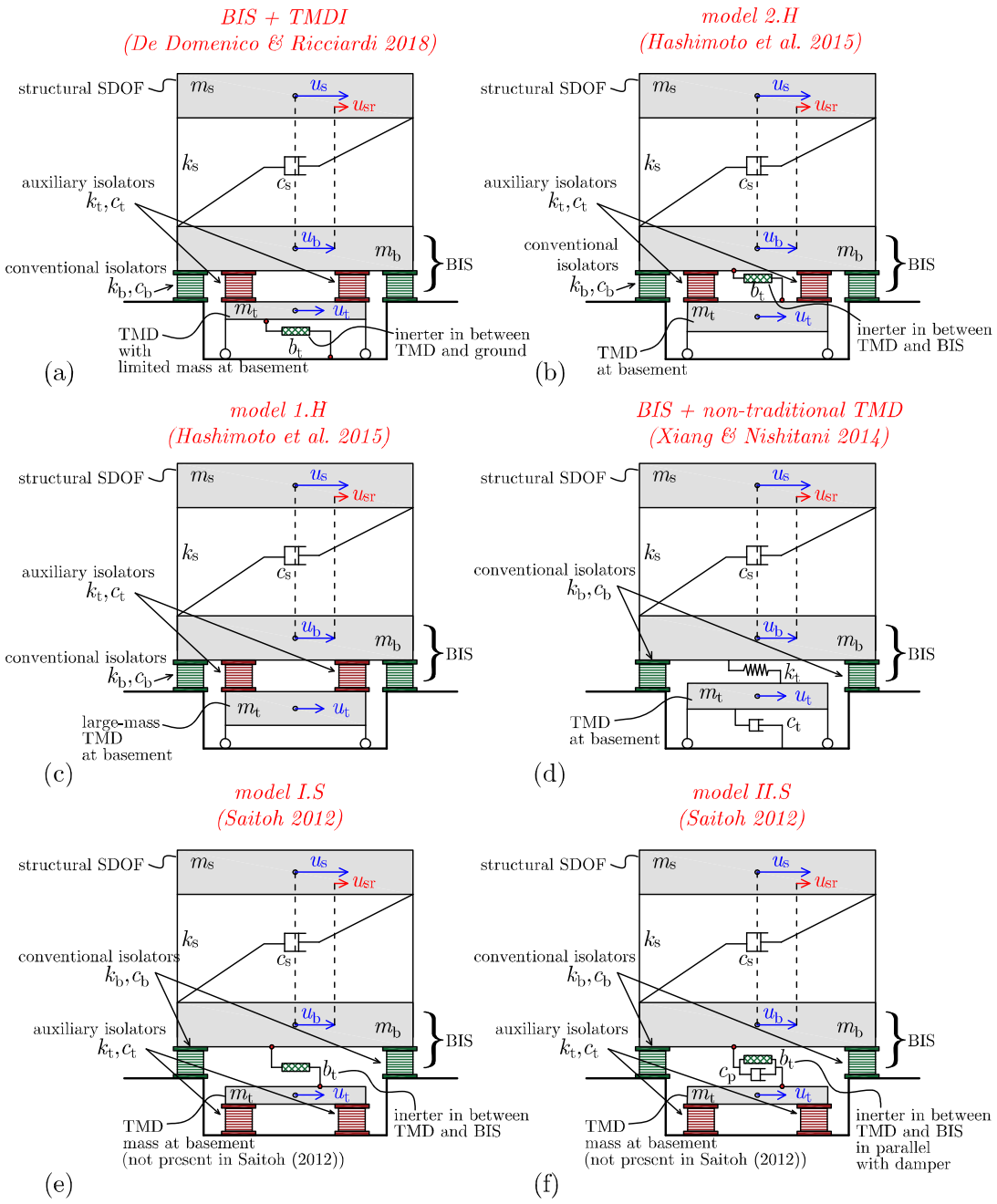

FIGURE 2 Six different structural control strategies for base-isolated structures combining tuned mass damper (TMD) and inertial dampers. BIS: base-isolation system

u_s relative to the ground, facilitates the extension to MDOF systems, as described in De Domenico and Ricciardi.[30] Although the same matrix–vector equation (3) is used for the six models, different definitions of the mass, damping, and stiffness matrices for each model are specified below.

The **M**, **C**, **K** matrices for the BIS + TMDI by De Domenico and Ricciardi[30] read

$$\mathbf{M} = \begin{bmatrix} m_s & m_s & 0 \\ m_s & m_s + m_b & 0 \\ 0 & 0 & m_{et} \end{bmatrix}; \quad \mathbf{C} = \begin{bmatrix} c_s & 0 & 0 \\ 0 & c_b + c_t & -c_t \\ 0 & -c_t & c_t \end{bmatrix}; \quad \mathbf{K} = \begin{bmatrix} k_s & 0 & 0 \\ 0 & k_b + k_t & -k_t \\ 0 & -k_t & k_t \end{bmatrix}, \tag{4}$$

where $m_{et} = m_t + b_t$ is the *effective* mass of the TMDI that incorporates both the physical mass m_t (of the TMD) and the apparent mass b_t (induced by the rotational inertia of the inerter). This model consists of a BIS with a TMDI attached at

the basement. The inertance b_t multiplies the relative acceleration between the TMD and the ground, that is, $\ddot{u}_t$. The case of BIS + TMD (without inerter) at the basement is retrieved from the previous matrices (4) for a zero value of b_t. The TMDI performance can therefore be improved by either increasing the TMD mass m_t or adjusting the gearing ratios of the inerter to attain higher inertance values b_t. However, the role of m_t and b_t is slightly different, as already noted in De Domenico and Ricciardi.[30]

A similar model was presented by Hashimoto et al[34] and named "Proposed-2 model" by the authors. This model is here labelled as model 2.H (H standing for the first author of the quoted paper), compare Figure 2. Unlike the previous system, in this model the inertial damper is not placed in between the TMD and the ground but is detached from the ground so as to reduce the corresponding reaction. The inerter was instead located in between the TMD and the isolation floor in order to reduce the TMD stroke. The relevant **M**, **C**, **K** matrices read

$$\mathbf{M} = \begin{bmatrix} m_s & m_s & 0 \\ m_s & m_s + m_b + b_t & -b_t \\ 0 & -b_t & m_{et} \end{bmatrix}; \quad \mathbf{C} = \begin{bmatrix} c_s & 0 & 0 \\ 0 & c_b + c_t & -c_t \\ 0 & -c_t & c_t \end{bmatrix}; \quad \mathbf{K} = \begin{bmatrix} k_s & 0 & 0 \\ 0 & k_b + k_t & -k_t \\ 0 & -k_t & k_t \end{bmatrix} \tag{5}$$

and differ from the ones in (4) only for the mass matrix, due to a different location of the inerter device that controls the relative displacements between TMD and BIS. The "Proposed-1 model" by Hashimoto et al[34] (here labelled model 1.H) is nothing but the above BIS with TMD at the basement and can be retrieved by Equation (5) for a zero value of b_t.

Xiang and Nishitani[10] studied a more effective TMD system for application to base-isolated structures. In an attempt to reduce the large TMD stroke, the dashpot associated with the TMD is not placed in parallel with the spring but is directly connected to the ground to mitigate the resonant behavior of the BIS. The resulting system was called "nontraditional TMD." The **M**, **C**, **K** matrices of the BIS + nontraditional TMD system are expressed as

$$\mathbf{M} = \begin{bmatrix} m_s & m_s & 0 \\ m_s & m_s + m_b & 0 \\ 0 & 0 & m_t \end{bmatrix}; \quad \mathbf{C} = \begin{bmatrix} c_s & 0 & 0 \\ 0 & c_b & 0 \\ 0 & 0 & c_t \end{bmatrix}; \quad \mathbf{K} = \begin{bmatrix} k_s & 0 & 0 \\ 0 & k_b + k_t & -k_t \\ 0 & -k_t & k_t \end{bmatrix}, \tag{6}$$

wherein the damping matrix is diagonal due to the particular location of the dashpot c_t.

Finally, for the displacement mitigation of base-isolated structures, Saitoh[33] elaborated various combined spring-damper-inerter configurations. In particular, the most complete and effective model was there called "model II," and here labelled model II. S, S standing for the initial of the author. It is formed by two units arranged in series: One unit is made of an inerter b_t and a dashpot c_p in parallel, which are directly connected to the BIS, whereas the other unit consists of a spring k_t and a damper c_t in parallel, which are here represented by an auxiliary set of isolators in line with the remainder of the paper, compare Figure 2. The mass m_t was not considered in the original model by Saitoh.[33] However, for consistency with all the other models, we here insert a TMD mass at the basement m_t similarly to all the other analyzed configurations. The **M**, **C**, **K** matrices for model II.S are

$$\mathbf{M} = \begin{bmatrix} m_s & m_s & 0 \\ m_s & m_s + m_b + b_t & -b_t \\ 0 & -b_t & m_{et} \end{bmatrix}; \quad \mathbf{C} = \begin{bmatrix} c_s & 0 & 0 \\ 0 & c_b + c_p & -c_p \\ 0 & -c_p & c_p + c_t \end{bmatrix}; \quad \mathbf{K} = \begin{bmatrix} k_s & 0 & 0 \\ 0 & k_b & 0 \\ 0 & 0 & k_t \end{bmatrix}. \tag{7}$$

It was found that the presence of the damper c_p in parallel with the inerter is effective to reduce the displacements induced by earthquake ground motions containing long-period components.[33] A simpler model, called model I.S, was also proposed without such damper c_p, compare Figure 2, and is basically retrieved from the former model II.S by setting $c_p = 0$ in (7).

Frequency, damping, and mass ratios of all the models presented above are expressed by exploiting the following positions:

$$\omega_s = \sqrt{\frac{k_s}{m_s}};\quad \omega_b = \sqrt{\frac{k_b}{m_b}};\quad \omega_t = \sqrt{\frac{k_t}{m_t + b_t}};\quad \zeta_s = \frac{c_s}{2\sqrt{m_s k_s}}; \zeta_b = \frac{c_b}{2\sqrt{m_b k_b}};\quad \zeta_t = \frac{c_t}{2\sqrt{(m_t + b_t)k_t}};$$
$$\zeta_p = \frac{c_p}{2\sqrt{m_b k_b}}; \mu_b = \frac{m_b}{m_s};\quad \mu_t = \frac{m_t}{m_s};\quad \beta_t = \frac{b_t}{m_s};\quad \mu_{et} = \frac{m_t + b_t}{m_s} = \frac{m_{et}}{m_s}. \tag{8}$$

The behavior of the six different models presented above is analyzed by examination of the frequency response functions (FRFs). From the above mass, damping, and stiffness matrices, and by assuming the ground acceleration as harmonic excitation $\ddot{u}_g(t) = e^{i\omega t}$, the response amplitude expressions for each structural control system are derived in closed form.

For the BIS + TMDI system by De Domenico and Ricciardi,[30] the FRFs are

$$U^{DR}_{u_{sr}}(\omega) = \frac{a_1 + \omega^4\mu_{et}\mu_t + a_2\mu_{et}(a_3 + \omega^2(1 + \mu_b + \mu_t))}{a_4 a_1 + \mu_{et}a_2(-\omega^4 + a_4 a_3)};$$
$$U^{DR}_{u_b}(\omega) = \frac{\mu_{et}a_2(a_4(1 + \mu_b) + \omega^2) - \mu_{et}\mu_t a_4(a_2 + \omega^2)}{a_4 a_1 + \mu_{et}a_2(-\omega^4 + a_4 a_3)}; \tag{9}$$
$$U^{DR}_{u_t}(\omega) = \frac{\mu_{et}(a_2 + \omega^2)(a_4(1 + \mu_b) - \omega^2) + \mu_t(a_4 a_3 - \omega^4)}{a_4 a_1 + \mu_{et}a_2(-\omega^4 + a_4 a_3)}.$$

For model II.H by Hashimoto et al,[34] the FRFs are

$$U^{H}_{u_{sr}}(\omega) = \frac{-a_5^2 + \omega^4\mu_t^2 + a_2\mu_{et}(a_3 + \omega^2(1 + \mu_b + \mu_t - \beta_t))}{-a_4 a_5^2 + \mu_{et}a_2(-\omega^4 + a_4(a_3 - \omega^2\beta_t))};$$
$$U^{H}_{u_b}(\omega) = \frac{\mu_{et}a_2(a_4(1 + \mu_b) + \omega^2) + \mu_t a_4 a_5}{-a_4 a_5^2 + \mu_{et}a_2(-\omega^4 + a_4(a_3 - \omega^2\beta_t))}; \tag{10}$$
$$U^{H}_{u_t}(\omega) = \frac{a_5(a_4(1 + \mu_b) + \omega^2) - \mu_t(\omega^4 + a_4\omega^2\beta_t - a_3 a_4)}{-a_4 a_5^2 + \mu_{et}a_2(-\omega^4 + a_4(a_3 - \omega^2\beta_t))}.$$

For the BIS + nontraditional TMD system by Xiang and Nishitani,[10] the FRFs are

$$U^{XN}_{u_{sr}}(\omega) = \frac{-\mu_{et}\omega_t^4 + \mu_t\omega^2\omega_t^2 + a_2(a_3 + \omega^2(1 + \mu_b) - 2i\omega\zeta_t\omega_t\mu_{et})}{-\mu_{et}\omega_t^4 a_4 + a_2(-\omega^4 + a_4(a_3 - 2i\omega\zeta_t\omega_t\mu_{et}))};$$
$$U^{XN}_{u_b}(\omega) = \frac{a_2(a_4(1 + \mu_b) + \omega^2) + \mu_t a_4\omega_t^2}{-\mu_{et}\omega_t^4 a_4 + a_2(-\omega^4 + a_4(a_3 - 2i\omega\zeta_t\omega_t\mu_{et}))}; \tag{11}$$
$$U^{XN}_{u_t}(\omega) = \frac{a_3 a_4 - \omega^4 - 2i\omega\zeta_t\omega_t\mu_{et}a_4 + (a_4(1 + \mu_b) + \omega^2)\omega_t^2}{-\mu_{et}\omega_t^4 a_4 + a_2(-\omega^4 + a_4(a_3 - 2i\omega\zeta_t\omega_t\mu_{et}))}.$$

Finally, for model II.S by Saitoh,[33] the FRFs are

$$U^{S}_{u_{sr}}(\omega) = \frac{a_6 a_7 + \omega^2\left(a_7(1 + \mu_b) - \left(\omega\beta_t - 2i\zeta_p\omega_b\mu_b\right)\left(\mu_{et}\omega - 2i\zeta_p\omega_b\mu_b\right)\right)}{-\omega^2\left(\omega\beta_t - 2i\zeta_p\omega_b\mu_b\right)^2 a_4 + (-\omega^4 + a_6 a_4)a_7};$$
$$U^{S}_{u_b}(\omega) = \frac{a_7\omega^2 + a_4(a_7(1 + \mu_b) - \omega\mu_t\left(\omega\beta_t - 2i\zeta_p\omega_b\mu_b\right)}{-\omega^2\left(\omega\beta_t - 2i\zeta_p\omega_b\mu_b\right)^2 a_4 + (-\omega^4 + a_6 a_4)a_7}; \tag{12}$$
$$U^{S}_{u_t}(\omega) = \frac{-\omega^4\mu_{et} + 2i\omega^3\zeta_p\omega_b\mu_b + a_4\left(a_6\mu_t - \omega(1 + \mu_b)\left(\omega\beta_t - 2i\zeta_p\omega_b\mu_b\right)\right)}{-\omega^2\left(\omega\beta_t - 2i\zeta_p\omega_b\mu_b\right)^2 a_4 + (-\omega^4 + a_6 a_4)a_7}.$$

In Equations (9)–(12), the following positions have been made to compact the notation:

$$
\begin{aligned}
&a_1 = \left(2\zeta_t\omega_t\mu_{et}\omega - \mathrm{i}\mu_{et}\omega_t^2\right)^2; \quad a_2 = -\omega^2 + 2\mathrm{i}\omega\zeta_t\omega_t + \omega_t^2;\\
&a_3 = -\omega^2(1+\mu_b) + \mu_b\omega_b^2 + \mu_{et}\omega_t^2 + 2\mathrm{i}\omega\left(\zeta_b\omega_b\mu_b + \zeta_t\omega_t\mu_{et}\right);\\
&a_4 = -\omega^2 + 2\mathrm{i}\omega\zeta_s\omega_s + \omega_s^2; \quad a_5 = \left(-\omega^2\beta_t + 2\mathrm{i}\omega\zeta_t\omega_t\mu_{et} + \mu_{et}\omega_t^2\right);\\
&a_6 = -\omega^2(1+\mu_b+\beta_t) + \mu_b\omega_b^2 + 2\mathrm{i}\omega\left(\zeta_b + \zeta_p\right)\omega_b\mu_b;\\
&a_7 = \mu_{et}\left(\omega_t^2 - \omega^2\right) + 2\mathrm{i}\omega\left(\zeta_p\omega_b\mu_b + \zeta_t\omega_t\mu_{et}\right).
\end{aligned}
\tag{13}
$$

Finally, the FRFs for the 2DOF uncontrolled BIS system (conventional BIS without any additional TMD or inertial damper) are

$$
\begin{aligned}
U_{u_{sr}}^U(\omega) &= \frac{\mu_b\omega_b(2\mathrm{i}\omega\zeta_b + \omega_b)}{-\omega^4 + \left(-\omega^2(1+\mu_b) + 2\mathrm{i}\omega\zeta_b\omega_b\mu_b + \mu_b\omega_b^2\right)\left(-\omega^2 + 2\mathrm{i}\omega\zeta_s\omega_s + \omega_s^2\right)};\\
U_{u_b}^U(\omega) &= \frac{-\omega^2\mu_b + \left(2\mathrm{i}\omega\zeta_s\omega_s + \omega_s^2\right)(1+\mu_b)}{-\omega^4 + \left(-\omega^2(1+\mu_b) + 2\mathrm{i}\omega\zeta_b\omega_b\mu_b + \mu_b\omega_b^2\right)\left(-\omega^2 + 2\mathrm{i}\omega\zeta_s\omega_s + \omega_s^2\right)},
\end{aligned}
\tag{14}
$$

the superscript U denoting the "uncontrolled" case. Note that the transfer functions of model I.H and of model I.S are special cases of those of models II.H and II.S, respectively, and can be retrieved from Equations (10) and (12) by setting $\beta_t = 0$ and $\zeta_p = 0$, respectively. Moreover, in the Xiang and Nishitani model described by Equation (11) (BIS + nontraditional TMD), $\mu_{et} \equiv \mu_t$ because no inerter is actually present.

In Figures 3 and 4, we have reported the amplitudes of the FRFs computed through Equations (9)–(14) for the six models and for the uncontrolled BIS. The following (arbitrary) parameters have been selected for the plots: $\zeta_s = 0.02$, $T_s = 0.5\,\mathrm{s}$, $\mu_b = 0.2$, $\zeta_b = 0.1$, $T_{b,\,\mathrm{eff}} = 2\,\mathrm{s}$, $\zeta_t = 0.2$, $T_t = 3\,\mathrm{s}$ (i.e., the auxiliary isolators are assumed to be slightly more

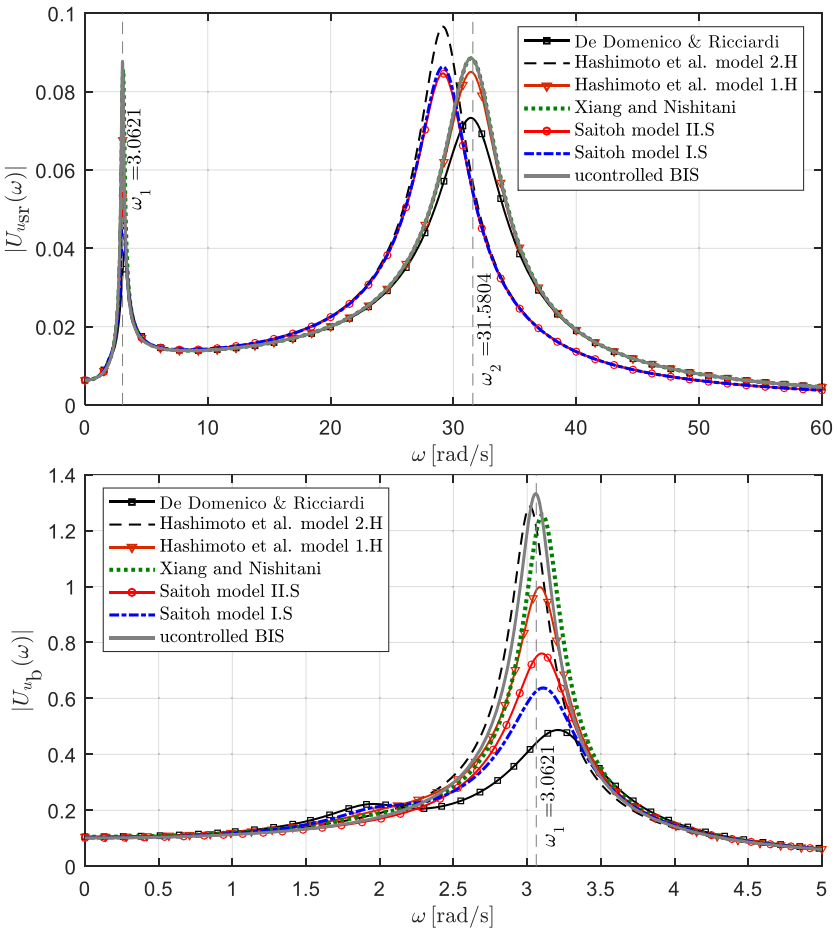

FIGURE 3 Amplitude of frequency response functions of displacements u_{sr} (top) and u_b (bottom) for $T_t = 3\,\mathrm{s}$, $\mu_t = 0.05$, and $\beta_t = 0.2$. BIS: base-isolation system

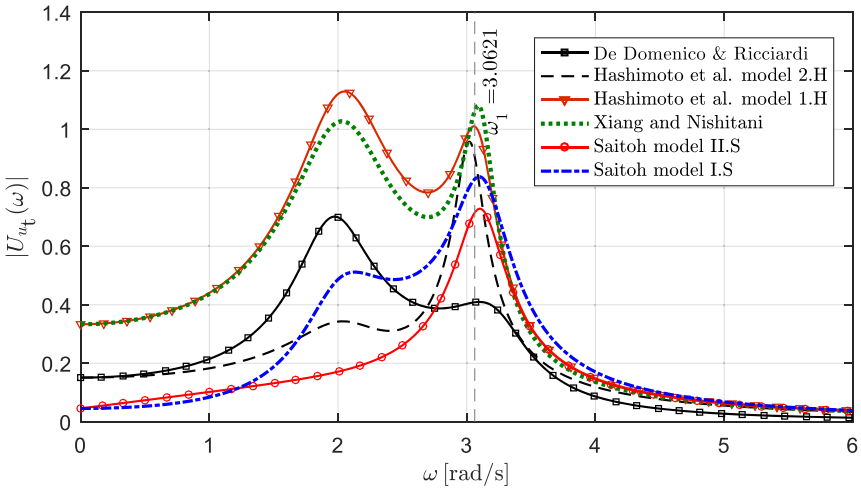

FIGURE 4 Amplitude of frequency response function of displacement u_t for $T_t = 3\,s$, $\mu_t = 0.05$, and $\beta_t = 0.2$

flexible than the conventional isolators), $\mu_t = 0.05$, $\beta_t = 0.2$, and $\zeta_p = 0.2$, where $T_s = 2\pi/\omega_s$, $T_{b,eff} = T_b\sqrt{1+\mu_b^{-1}}$ with $T_b = 2\pi/\omega_b$ and $T_t = 2\pi/\omega_t$ (note that the frequency ratio $\omega_t/\omega_b \approx 0.27$ for the selected parameters). For the selected parameters, the BIS + TMDI model by De Domenico and Ricciardi is the most effective structural control system for reducing both the displacement response amplitudes $|U_{u_{sr}}(\omega)|$ and $|U_{u_b}(\omega)|$ in comparison with the uncontrolled BIS. The two models by Saitoh reduce the displacement response amplitude $|U_{u_b}(\omega)|$ quite well and are also effective with regard to the TMD displacement, namely, the amplitude $|U_{u_t}(\omega)|$, compare Figure 4. The poor performance of the model by Xiang and Nishitani is strictly related to the chosen value of T_t and μ_t as will be clarified below. Finally, the two models by Hashimoto et al are not correctly tuned for reducing the displacement response amplitudes for this specific set of parameters. Note that model 2.H leads to a lower response amplitude $|U_{u_t}(\omega)|$ than model 1.H due to the presence of the inerter β_t placed in between the TMD and the BIS. The effect of β_t can also be examined by comparing the BIS + TMDI model with model 1.H, which is basically the same model without inerter between the TMD and the ground, compare the sketches in Figure 2.

The discussed behaviors are highly dependent on the chosen dynamic parameters. The comparison between the six models should be made with reference to optimal TMD parameters that may be different from the ones adopted in the previous graphs. As an example, in Figure 5, we report the amplitudes of the FRFs of u_{sr} and u_b in the case of $T_t = 2\,s$ (auxiliary isolators as flexible as the conventional isolators), $\mu_t = 0.1$, and $\beta_t = 0.05$, whereas the other parameters are kept the same as above. In this case, the frequency ratio $\omega_t/\omega_b \approx 0.40$. It is seen that the variation of the mass and inertance ratios yields a different behavior of the systems: The BIS + TMDI still remains the most effective system for reducing the amplitude $|U_{u_{sr}}(\omega)|$ (although models II.S and 1.H attain a comparable performance). However, as compared to the previous set of parameters, there is a considerable improvement of the two models by Hashimoto et al and of the model by Xiang and Nishitani with regard to the u_b reduction. This means that the optimal frequency ratio for these models is closer to $\omega_t/\omega_b \approx 0.40$ than to $\omega_t/\omega_b \approx 0.27$. The different combination of μ_t and β_t also results in a different behavior in terms of $|U_{u_t}(\omega)|$ amplitude. From Figure 6, it seems that the two models by Saitoh perform considerably better the other ones; it will be demonstrated below via time-history analyses that model II.S is the best one with regard to TMD-related response. Moreover, both models by Hashimoto et al and the model by De Domenico and Ricciardi amplify the $|U_{u_t}(\omega)|$ amplitude as compared to the previous case. Indeed, these models need higher inertance ratios β_t than 0.05 to reduce the displacement u_t and the resulting TMDI stroke, as will be clarified in the optimal design graphs presented in the next section.

A preliminary tuning procedure for selecting the most appropriate frequency ratio ω_t can be obtained by examining the natural frequencies of the *undamped* system (without damping). The first two natural frequencies ω_1, ω_2 are related to the dynamic properties of the BIS and the TMD, whereas ω_3 is related to the superstructure (because $\omega_s \gg \omega_b$). In Figure 7, such first two frequencies, normalized by ω_{bu} (i.e., the natural frequency related to the BIS in the uncontrolled system), are plotted against the frequency ratio $\nu_t = \omega_t/\omega_b$ for the two sets of mass and inertance ratios chosen above. There exists a particular value of the frequency ratio ν_t (near 0.4) for which the first two undamped frequencies ω_1 and ω_2 are close to each other. If the TMD is selected according to this ν_t ratio, the BIS and the TMD are tuned optimally. As we will see below, this particular frequency ratio is close to the optimal tuning of the TMD to reduce the displacement response of the base-isolated structure.

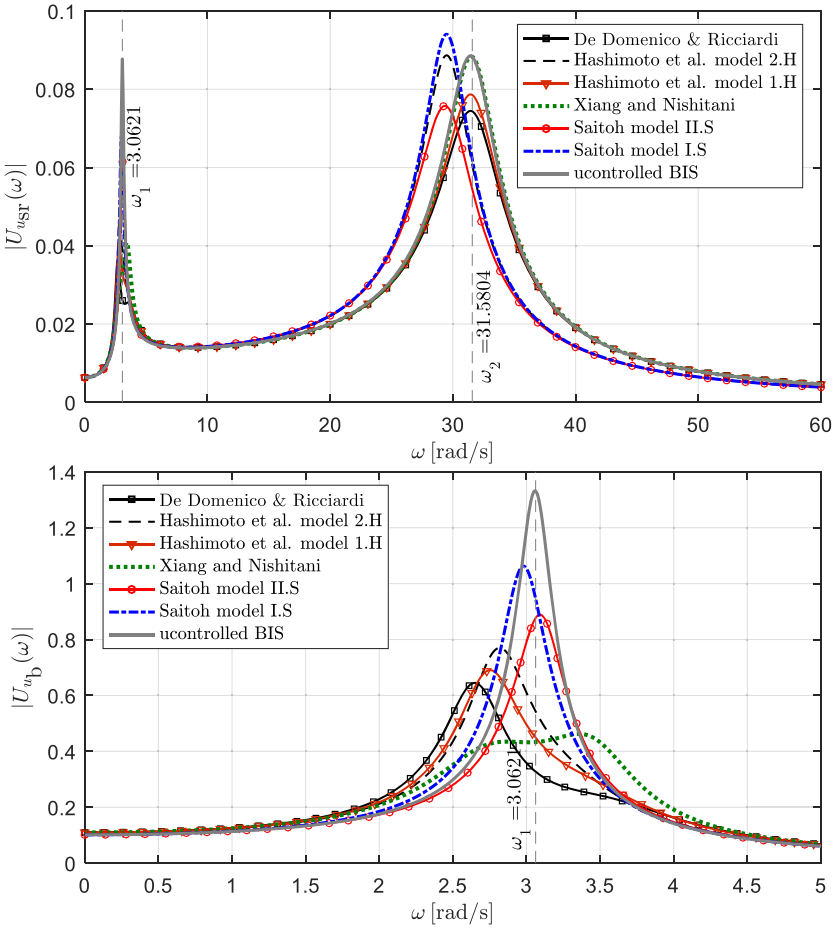

FIGURE 5 Amplitude of frequency response functions of displacement u_{sr} (top) and u_b (bottom) for $T_t = 2\,s$, $\mu_t = 0.1$, and $\beta_t = 0.05$. BIS: base-isolation system

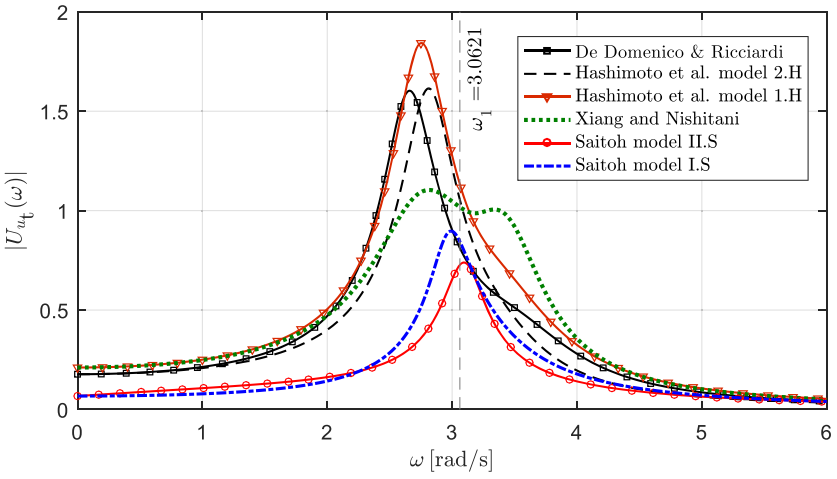

FIGURE 6 Amplitude of frequency response function of displacement u_t for $T_t = 2\,s$, $\mu_t = 0.1$, and $\beta_t = 0.05$

4 | OPTIMAL DESIGN AND TUNING PROCEDURE

From the previous comparison of the FRFs, it has been highlighted that the six models lead to completely different dynamic performances for the same set of input parameters. Indeed, although the mass, damping, and frequency ratios are the same, the different arrangement of mass-spring-dashpot-inerter elements leads to a dynamic behavior that varies from model to model. Therefore, a consistent comparison of the six models should be made provided the optimal parameters of each model are preliminarily identified. These optimal parameters are expected to be different from

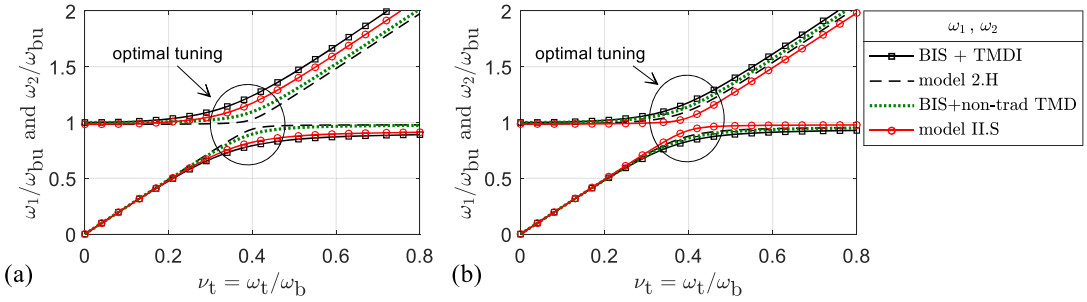

FIGURE 7 First two undamped natural frequencies of the assembled systems for $\omega_b/\omega_s = 0.2$ and $\mu_b = 0.2$: (a) $\mu_t = 0.05$ and $\beta_t = 0.2$; (b) $\mu_t = 0.1$ and $\beta_t = 0.05$. BIS: base-isolation system; TMD: tuned mass damper; TMDI: tuned mass damper inerter

model to model and depends on the placement of the aforementioned elements within the structure. This section aims to provide guidelines on the selection of the optimal design parameters of each model based on a common, unified strategy. In line with other studies in the literature, some parameters are the free design variables sought in the optimization problem, while other parameters are supposed known. We assume that the base-isolated structure is characterized by the following (benchmark) parameters: $\zeta_s = 0.02$, $T_s = 0.5\,\text{s}$, $\mu_b = 0.2$, $\zeta_b = 0.1$, and $T_{b,\text{eff}} = 2\,\text{s}$. The choice of a low damping ratio for the BIS, implying the use of elastomeric isolators, is motivated by earlier studies regarding the performance of the BIS + TMDI system.[30] The TMD/TMDI subsystem is characterized by five parameters in the most general case, collected in the vector $\mathbf{x}_{\text{param}} = \{\omega_t, \zeta_t, \mu_t, \beta_t, \zeta_p\}$. Among these five parameters, the design process aims to find the optimal set of design parameters $\mathbf{x}_d$ (e.g., the optimal couple $\mathbf{x}_d = \{\nu_t, \zeta_t\}$, with $\nu_t = \omega_t/\omega_b$), associated with a chosen set of free parameters (e.g., $\mathbf{x}_{\text{free}} = \{\mu_t, \beta_t, \zeta_p\}$). The goal is to find the best set of $\mathbf{x}_d$ that minimizes a performance index, that is, a representative measure of the system response. In mathematical terms, a nonlinear constrained single-objective multivariable optimization problem is addressed in the form

$$\min_{\mathbf{x}_d} f(\mathbf{x}_d) \quad \text{such that } \mathbf{x}_{d,lb} \le \mathbf{x}_d \le \mathbf{x}_{d,ub}, \tag{15}$$

where $f(\mathbf{x}_d)$ is the chosen objective function (OF) to minimize and $\mathbf{x}_{d,lb}$ and $\mathbf{x}_{d,ub}$ are the lower bound and upper bound vectors of the design variables, respectively.

Owing to the stochastic nature of earthquake ground motion,[36] the base acceleration $\ddot{u}_g(t)$ is assumed as a Gaussian zero-mean white-noise stationary random process for a simplified optimization procedure.[30] Transient nonstationary phenomena, which may cause degradation of performance of the inerter,[37] are neglected here. Typical input–output relationships in the frequency domain are employed to determine the covariance matrix of the system response $\Sigma_{\mathbf{uu}} = \text{E}[\mathbf{u}\mathbf{u}^T]$, with $\text{E}[\cdot]$ denoting the expectation operator, that is,

$$\Sigma_{\mathbf{uu}} = \begin{bmatrix} \sigma^2_{u_{sr}} & \sigma_{u_{sr}u_b} & \sigma_{u_{sr}u_t} \\ \sigma_{u_{sr}u_b} & \sigma^2_{u_b} & \sigma_{u_b u_t} \\ \sigma_{u_{sr}u_t} & \sigma_{u_b u_t} & \sigma^2_{u_t} \end{bmatrix} \tag{16}$$

that contains the variances of the three displacements along the main diagonal, and the cross-covariances of the displacement response in the off-diagonal terms.

The optimization problem (15) is handled via a numerical search algorithm, through the built-in MATLAB *fmincon* function, as described in De Domenico and Ricciardi.[30] The optimum design variables $\mathbf{x}_d$ are found by minimization of the variance of the displacement $u_s = u_{sr} + u_b$, that is, the OF is

$$\text{OF} = \sigma^2_{u_s} = \text{E}\left[u_s^2\right] = \sigma^2_{u_{sr}} + \sigma^2_{u_b} + 2\sigma_{u_{sr}u_b}. \tag{17}$$

In addition to the variance of the displacement u_s, in the sequel also the variance of the total acceleration $\ddot{u}_{s,\text{tot}} = \ddot{u}_{sr} + \ddot{u}_b + \ddot{u}_g$ is computed. It is worth noting that the latter response indicator is related to the forces arising in the superstructure.[30] Therefore, minimizing the total acceleration is also related to minimizing the interstory displacement relative to the BIS, which is associated with the stress in the superstructure and is a relevant quantity of interest to assess the performance of a structural control system. Additionally, also the variance of the TMD stroke $u_{tb} = u_t - u_b$ is computed in order to assess the effectiveness with regard to the structural system as a whole. Indeed,

large values of $\sigma^2_{u_{tb}}$ mean that a large space in the building should be devoted to the secondary mass to accommodate the TMD displacements. This response indicator is often the governing quantity for the applicability of the TMD strategy, as confirmed by previous studies in the field of TMD tuning.[38]

A wide family of design graphs are presented in this section for the optimal design of the six structural control systems. The following normalized response indicators are introduced:

$$\begin{aligned} f_1 &= \frac{\sigma^2_{u_s}}{\sigma^2_{u_{s0}}} \quad \text{normalized displacement variance} \\ f_2 &= \frac{\sigma^2_{\ddot{u}_{s,tot}}}{\sigma^2_{\ddot{u}_{s0,tot}}} \quad \text{normalized total acceleration variance} \\ f_3 &= \frac{\sigma^2_{u_{tb}}}{\sigma^2_{u_{b0}}} \quad \text{normalized TMDI stroke variance,} \end{aligned} \tag{18}$$

wherein the adjective "normalized" means that the quantities are divided by the same measure calculated in the uncontrolled BIS (without any additional TMD-based system). An effective structural control strategy should lead to response ratios f_1, f_2, f_3 lower than the unity.

In Figure 8, the design graphs that are relevant to the BIS + TMDI are illustrated. Different curves are shown, each one related to a fixed effective mass ratio μ_{et} as a combination of μ_t and β_t, where β_t is reported in the horizontal axis, whereas six values of the μ_t ratio are investigated, corresponding to six different curves. The case $\mu_t = 0$ is representative of the TID, while the traditional TMD (without inerter) is retrieved at the intersection with the vertical axis, that is, for $\beta_t = 0$. It is seen that the performance is improved by increasing either β_t or, similarly, μ_t. Displacement and acceleration reductions corresponding to $f_1 \approx 0.4$ and $f_2 \approx 0.4$ (associated with reductions of the order of 60%) can be attained by the TID ($\mu_t = 0$) with an inertance ratio $\beta_t \approx 0.1$. Nevertheless, in order to reduce the TMDI stroke as compared to the uncontrolled BIS, higher values than $\beta_t = 0.2$ are necessary, as shown in Figure 8c)—a thicker solid horizontal line has been drawn to distinguish between amplification and reduction. Lower inertance values results in a considerable amplification of the TMDI stroke. For the limit case of the TMD ($\beta_t = 0$), mass ratios that are higher than $\mu_t = 0.5$ would be necessary to prevent stroke amplification. This confirms the more beneficial effect induced by the inertance over the mass, especially in terms of control of the TMD displacement, which is in line with Pietrosanti et al.[24] The optimal TMD frequency parameter ν_t monotonically decreases by increasing μ_t and β_t, whereas an opposite trend is observed for the damping parameter ζ_t that increases with increasing μ_t and β_t.

In Figure 9, the design graphs for models 2.H and 1.H (the latter retrieved for the limit case $\beta_t = 0$) are presented. It is verified that model 1.H coincides with the above BIS + TMDI model with a value $\beta_t = 0$; indeed, the two models

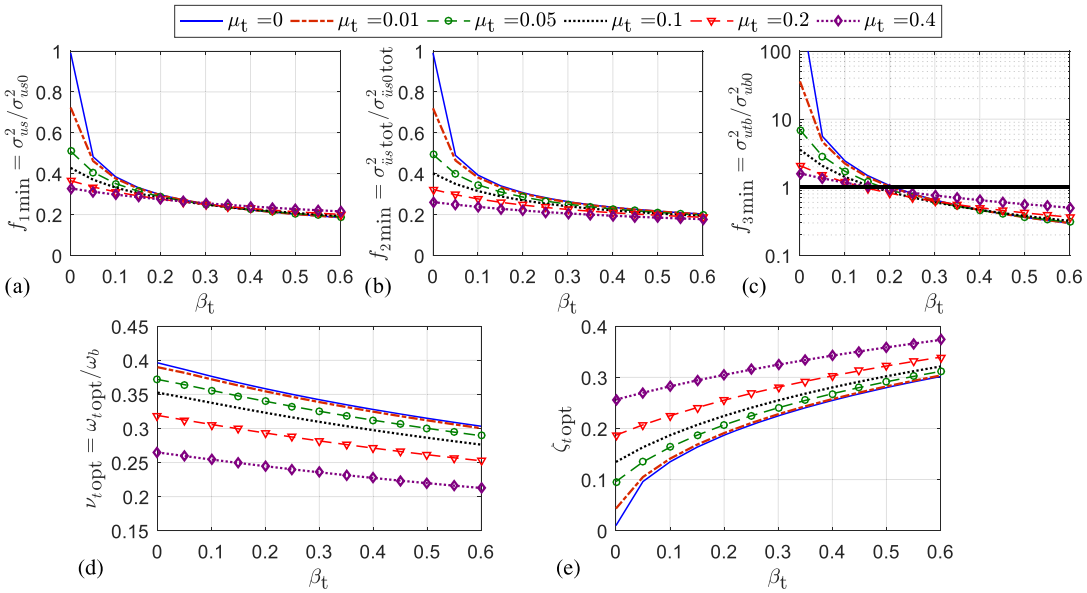

FIGURE 8 Optimal design and performance evaluation of base-isolation system + tuned mass damper inerter system

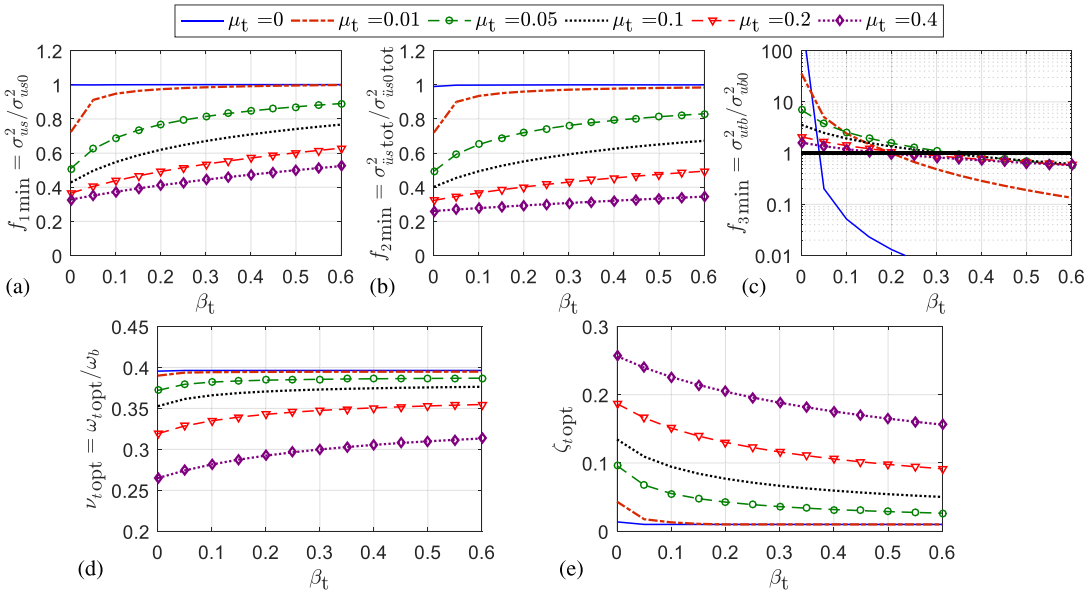

FIGURE 9 Optimal design and performance evaluation of models 1.H and 2.H

provides the same optimal parameters at the intersection with the vertical axis. Increasing the TMD mass μ_t monotonically reduces both the displacement and acceleration response ratios f_1, f_2. Instead, the role of the inertance β_t is different from that of the BIS + TMDI system discussed above: increasing β_t leads to higher values of f_1, f_2. On the other hand, increasing β_t yields a reduction of the normalized TMDI stroke variance, compare Figure 9c). Without inerter ($\beta_t = 0$), even for extremely large mass ratios $\mu_t = 0.5$, the TMDI stroke amplification cannot be prevented. This is consistent with the dynamic layout of model 2.H, in which the inerter is not directly attached to the ground (like in the BIS + TMDI model) but is placed in between the TMD and the BIS, thus controlling the TMDI stroke $u_{tb} = u_t - u_b$. A reasonable, though expensive, choice could be the couple $(\mu_t, \beta_t) = (0.4, 0.4)$ that guarantees f_1, f_2, f_3 ratios lower than the unity. Moreover, the optimal TMD parameters ν_t, ζ_t follow a similar trend to that of the BIS + TMDI model with regard to the mass ratio μ_t, but an opposite trend with regard to the inertance ratio β_t, due to the different placement of the inerter.

In the BIS + nontraditional TMD, whose relevant design graphs are depicted in Figure 10, the optimal frequency ratio ν_t for fixed damping and mass ratios ζ_t, μ_t, respectively, is identified. Six different ζ_t ratios are explored and a family

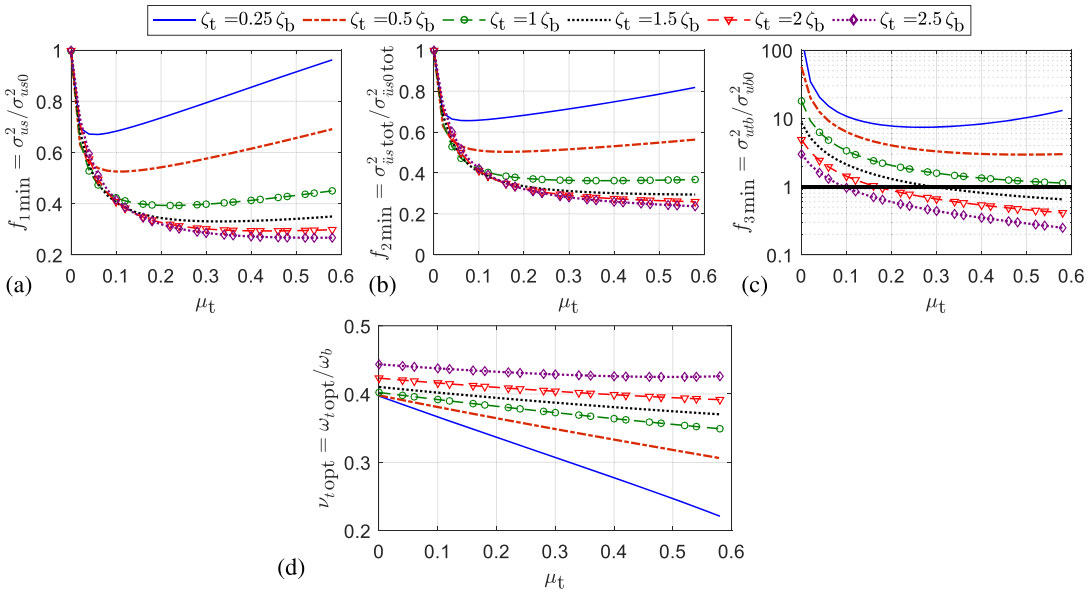

FIGURE 10 Optimal design and performance evaluation of base-isolation system + nontraditional tuned mass damper system

of mass ratios ranging from 0 to 0.6. The performance in terms of f_1, f_2 is improved with increasing mass ratios μ_t only for damping ratios $\zeta_t > \zeta_b$, whereas the f_1, f_2 curves for $\zeta_t < \zeta_b$ exhibit a concave profile with an optimum mass ratio near $\mu_t = 0.05$ for the selected parameters. Effective reduction of the normalized TMDI stroke can be accomplished only for $\zeta_t > \zeta_b$, in a range of mass ratios that increases with increasing ζ_t. The optimal TMD frequency parameter ν_t moderately decreases with increasing μ_t and increases with increasing ζ_t.

Finally, the design graphs for models I.S and II.S are plotted in Figures 11 and 12, respectively. In particular, for model I.S, the optimal inertance ratio β_t is identified for a given TMD frequency ratio $\nu_t = 0.4$, for six different damping ratios ζ_t and for a family of mass ratios μ_t ranging from 0 to 0.6. Saitoh[33] did not consider the TMD mass ($\mu_t = 0$) in his original model, and this configuration can be retrieved at the intersection with the vertical axis. High optimal inertance ratios are found, of the order $\beta_t = 0.5 - 1.0$ (Saitoh[33] considered a value $\beta_t = 1.0$). Although reductions of displacements and accelerations are guaranteed throughout the range of investigated parameters (f_1, f_2 ratios <1), normalized TMDI stroke reductions can be obtained either with $\zeta_t > 1.5\zeta_b$ or with a combination of $\zeta_t < 1.5\zeta_b$ with large mass ratios μ_t. For model II.S, the optimal damping parameter ζ_p is identified for a given TMD frequency ratio $\nu_t = 0.5$ and damping ratio $\zeta_t = \zeta_b$, see Figure 12. In this case, effective reductions of all the three response indicators can be achieved with $\beta_t > 0.1$. The optimal ζ_p increases with increasing β_t and also with increasing μ_t.

All the above graphs are developed for SDOF primary structures. Strictly speaking, accurate tuning procedures of TMD for MDOF systems should include the effects of more than only one mode of vibration, see for example, Krenk and Høgsberg.[39] An effective tuning procedure of TMD accounting for different modes was also proposed in Bortoluzzi et al[14] and Casciati et al[40] to mitigate wind-induced local, rather than global, vibrations in bridges. In the latter cases, appropriate reduced-order models are preliminarily necessary[41,42] so as to reduce the computational effort before the tuning procedure. Although all these more accurate procedures are preferable, most of the literature studies dealing with the TMD tuning address only a single mode of vibration in a simplified way, especially in the context of framed buildings and earthquake excitations like the ones considered in this paper, see, for example, previous studies.[23,26,43-47] A simplified way to extend the optimal design of the TMD to MDOF systems, which neglects the higher order modes of the superstructure, has been described in De Domenico et al[31] and is adopted here.

5 | TIME-HISTORY ANALYSIS AND COMPARISONS

In this section, the dynamic performance of the aforementioned six structural control strategies is scrutinized in the time domain. In particular, the same five-story planar frame building previously analyzed in De Domenico and Ricciardi[30] (refer to fig. 13 in De Domenico and Ricciardi[30]) is here considered. Mechanical and geometric parameters are fully described in De Domenico and Ricciardi.[30] In this regard, it is worth making some remarks about this

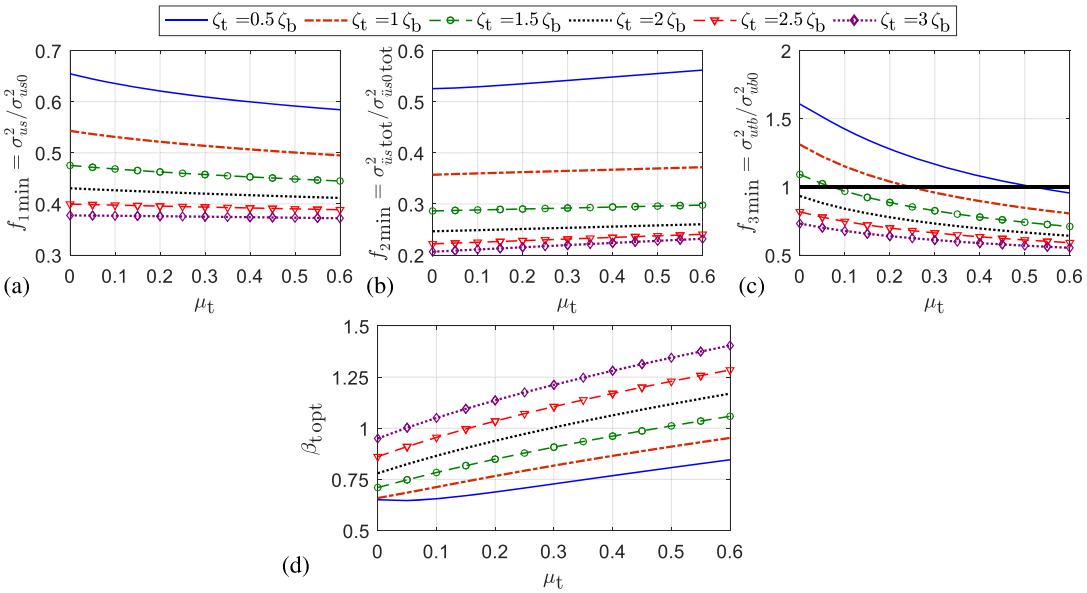

FIGURE 11 Optimal design and performance evaluation of model I.S with $\omega_t = 0.5\omega_b$

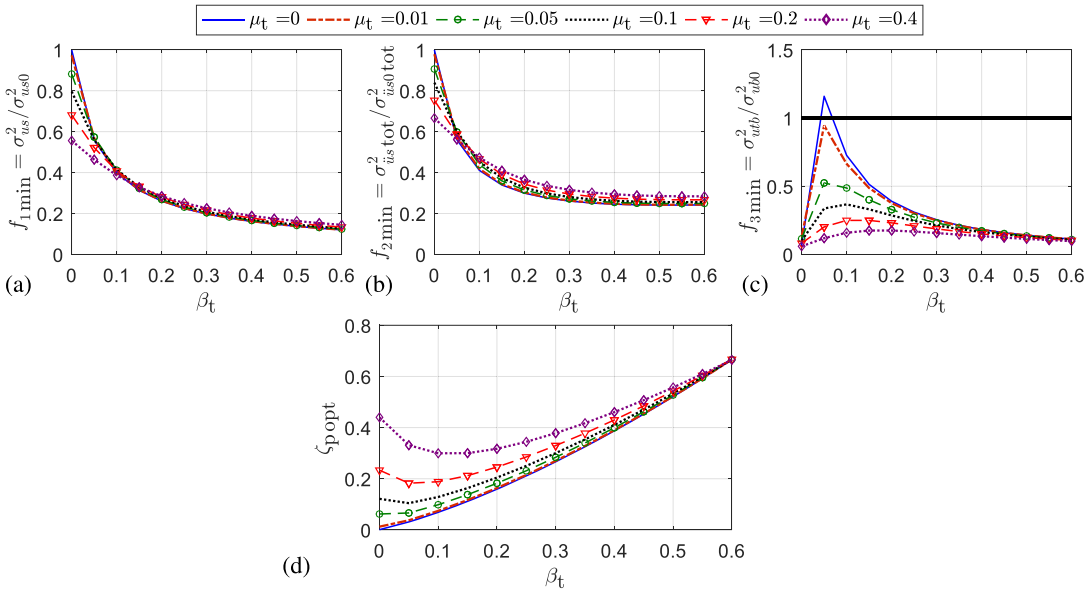

FIGURE 12 Optimal design and performance evaluation of model II.S with $\omega_t = 0.5\omega_b$ and $\zeta_t = \zeta_b$

simplified planar model: (a) In most base-isolation projects of new construction, the stiffness characteristics of the isolators are selected so as to lead to minimal eccentricity between the centers of mass and stiffness of the structure, thereby minimizing torsional effects; (b) even in existing buildings that are asymmetrical, the isolators may be designed and tailored so as to accomplish the above mentioned effect. Although it is well known from experimental findings that seismic isolators are very sensitive to the bidirectional nature of the ground motion,[48] the focus of this paper is to compare different structural control layouts involving TMD and inerter devices. It is restricted to this main scope that the adopted simplified two-dimensional schematization of the structure should be meant. It is believed that planar structural models can offer significant computational efficiency while not majorly prejudicing the generality of the following discussions and comparisons in place of alternative more accurate but cumbersome 3D analyses.

This considered building is meant as an ordinary reinforced concrete[49,50] base-isolated structure, with an additional structural control strategy implemented underneath the base-isolation floor. The choice of this building, which has been investigated in earlier research work by the authors[30] with regard to the BIS + TMDI, is motivated by the possibility of comparing results already published in the literature with alternative control techniques. The frame building has a first natural period $T_1 \cong 0.50\,\mathrm{s}$; the damping coefficients of the superstructure are assumed to be stiffness-proportional ("classically damped system") with $\zeta_s = 0.02$ for all the vibration modes. The base-isolation floor is assumed to have mass $m_b = 47500\,\mathrm{kg}$. The first effective modal mass[51] for the building is $m_1^* = 2.3714{\times}10^5\,\mathrm{kg}$, representing the 81.7% of the total mass of the building. This results in a mass ratio $\mu_b = m_b/m_1^* \cong 0.20$. The BIS is assumed to have $\zeta_b = 0.1$ and effective natural period $T_{b,\mathrm{eff}} = 2\,\mathrm{s}$. Note that all the above numerical data are purposely chosen to be perfectly consistent with the parameters adopted in Section 4 for drawing the design graphs. Therefore, such design graphs can be referred to for the selection of the optimal TMD parameters.

The design process is articulated in the following steps: (a) choose some reasonable values of $\mathbf{x}_{\mathrm{free}}$ parameters so that there exists a possible combination of the remaining $\mathbf{x}_d$ design TMD parameters such that all the three response indicators f_1, f_2, f_3 are lower than the unity; (b) evaluate the best combination of $\mathbf{x}_d$ design parameters that minimizes the chosen OF via the developed design graphs. Considering the design graphs of Section 4, in all the models, μ_t and β_t are free parameters (obviously in model 1.H and in the BIS + nontraditional TMD the ratio $\beta_t = 0$). As an exception, β_t is a design parameter in model I.S. Furthermore, ζ_t is a free parameter in the BIS + nontraditional TMD. In models I.S and II.S, both ω_t and ζ_t are free parameters, because the TMD is grounded in this case.

In an attempt to make a consistent comparison among the six models, the TMD design parameters have been selected based on values of the response ratios f_1, f_2, f_3 ranging from 0.25 to 0.8, which serves as a criterion for selecting consistent parameters. The detected optimal parameters are reported in Table 1. The uncontrolled BIS, that is, the conventional BIS without any additional structural control strategy, is also considered as reference solution. It is quite difficult to obtain identical f_1, f_2, f_3 ratios for all the models. Moreover, the little differences should be interpreted considering the

TABLE 1 Selection of the TMD parameters for the six structural control strategies of this study

Structural control strategy	μ_t	β_t	ν_t	ζ_t	ζ_p	f_1	f_2	f_3
Conventional BIS	-	-	-	-	-	1.00	1.00	1.00
BIS + TMDI	0.01[a]	0.3[a]	0.339[b]	0.228[b]	-	0.25	0.26	0.64
Model 2.H	0.4[a]	0.4[a]	0.306[b]	0.175[b]	-	0.47	0.32	0.72
Model 1.H	0.4[a]	-	0.265[b]	0.256[b]	-	0.33	0.26	1.60
BIS + nontraditional TMD	0.2[a]	-	0.447[b]	0.25[a]	-	0.32	0.31	0.52
Model I.S	0[a]	0.86[b]	0.5[a]	0.25[a]	-	0.40	0.22	0.82
Model II.S	0[a]	0.2[a]	0.5[a]	0.1[a]	0.261[b]	0.26	0.30	0.39

Note. BIS: base-isolation system; TMD: tuned mass damper; TMDI: tuned mass damper inerter

[a]Free parameter (assumed based on the design graphs developed in Section 4).

[b]Design parameter (calculated by minimization of the displacement variance).

assumption of ground motion modelled as a stationary white-noise random process. Because earthquake ground motions are neither stationary nor have a uniform spectral content as represented by the white-noise model, these differences are only qualitative. It is of interest to assess the performance of the six models via time-domain analyses with real accelerograms. These more realistic analyses serve to assess the validity of the simplified optimal design procedure described in Section 4 considering real accelerograms that are neither Gaussian nor stationary.

As a first step, the same set of eight natural earthquake ground motions considered in De Domenico and Ricciardi[30] are used for the response-history analysis (see table 1 and fig. 8 of the quoted paper[30] for more specifications on these earthquakes). In line with the indications outlined in Giuliano,[15] this group of accelerograms comprise both near-fault ground motions, with long-period fling pulse, and far-field ground motions, which tend to have a fairly smooth transition of temporal and spectral contents.[8,10] Besides this first group of eight accelerograms, a larger number of samples, belonging to the FEMA P695 far-field record set,[52] is subsequently analyzed to draw more general conclusions over a wider set of seismic inputs. In order to separate the intensity factor and to focus on the record-to-record variability ascribed to the different frequency content and impulsive character of the considered accelerograms, the recorded ground motions have been scaled by a common scale factor, assumed as the displacement of the BIS ($u_b = 20\,\text{cm}$), see, for example, Castaldo and Ripani.[53] This does not affect the results significantly but is helpful to reduce the variability of the response caused by the different intensity levels, which is a secondary aspect for this study as all the considered systems are linearized.

Time-history response of the base-isolated building is calculated by direct integration of the equations of motion. As an example, the time-history response in terms of base shear V_b, last-floor displacement relative to the ground $u_{s5} = u_{sr5} + u_b$, and the TMD stroke $u_{tb} = u_t - u_b$ are reported in Figure 13 for two accelerograms, namely, L'Aquila and Loma Prieta. It is clear that these two ground motions have quite different characteristics. In particular, the former has a high impulsive content in the first instants of motion; therefore, there is no time for the transfer of energy from the base-isolated structure to the TMD. Indeed, the first peak, which is the most important one for this specific ground motion, is not damped by any structural control strategy. On the contrary, the time-history response under the Loma Prieta earthquake shows a gradual transfer of energy from the seismic input and the TMD, so that the TMD-related control strategy is much more effective in this case. However, it is expected that in both cases, the root-mean-square (rms) values of the response (over the entire time-history duration) is considerably reduced as compared to the conventional BIS case. To quantify this reduction, in Table 2, the rms values of a few superstructure response indicators, averaged on the eight accelerograms, are listed. The quantities called kinetic energy and elastic strain energy of the superstructure are calculated as $T_s = \frac{1}{2}\dot{\mathbf{u}}_s^T \mathbf{M}_s \dot{\mathbf{u}}_s$ and $E_s = \frac{1}{2}\mathbf{u}_{sr}^T \mathbf{K}_s \mathbf{u}_{sr}$, respectively, see Salvi and Rizzi,[43] and are representative scalar measures of the overall stress and strain occurring in the superstructure. In Table 2, the percentages of reductions of each quantities as compared to the conventional BIS are reported in brackets. Note that the deterministic rms values are related to the variances in the probabilistic framework. These reductions are rather comparable in the six models, thus confirming that the TMD parameters reported in Table 1 are reasonably chosen for a consistent comparison. As an example, the rms base shear is halved in almost all the models. The best performance in terms of reductions of rms superstructure-related response indicators is attained by the BIS + TMDI model, except for the reductions of the total accelerations for which models 2.H and 1.H and the BIS + nontraditional TMD are slightly better. On the contrary,

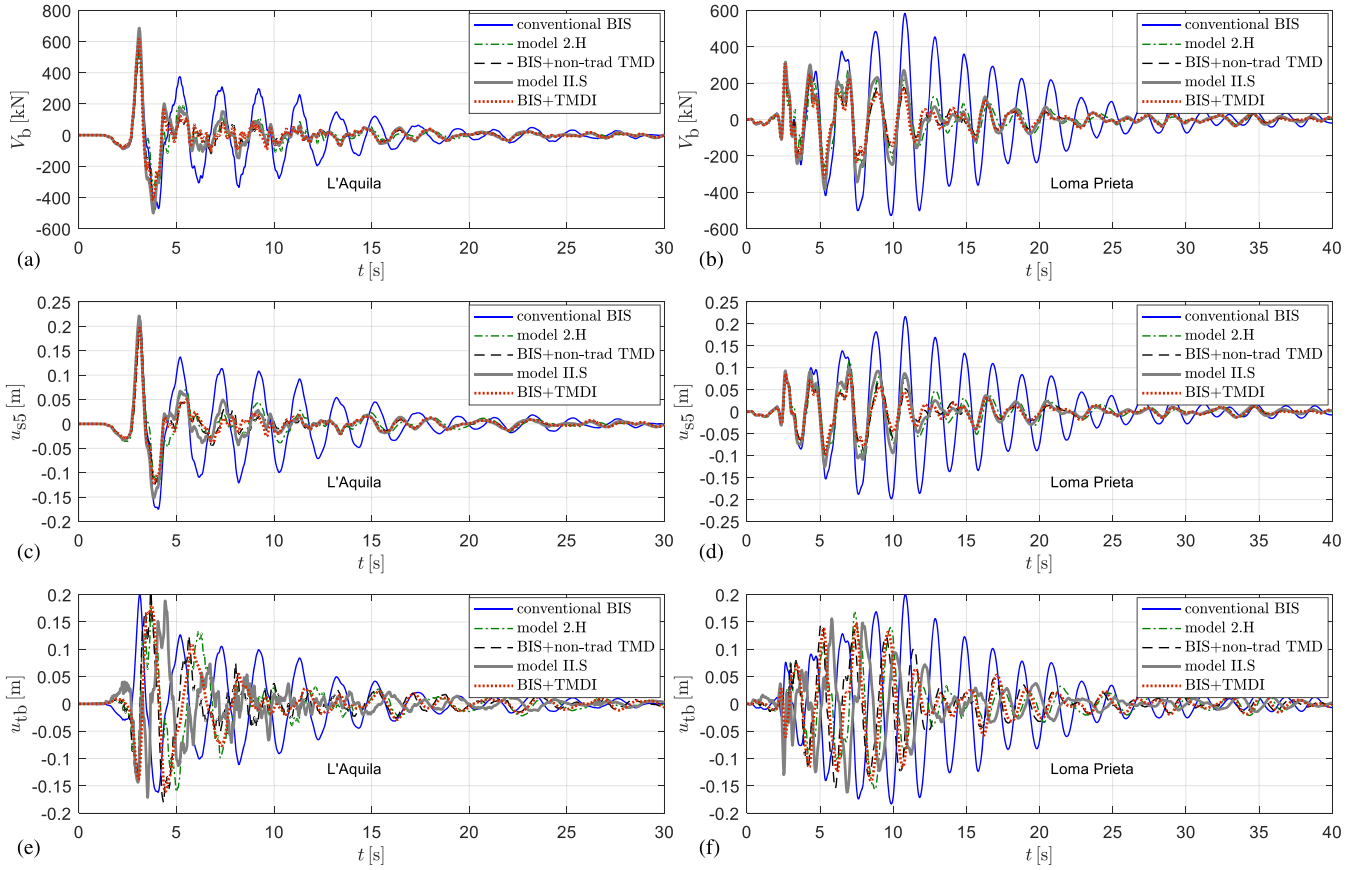

FIGURE 13 Time-history response of the base-isolated building subject to natural earthquake ground motions of L'Aquila and Loma Prieta: (a–b) base shear; (c–d) last-floor displacement; (e– f) TMD stroke. BIS: base-isolation system; TMD: tuned mass damper; TMDI: tuned mass damper inerter

TABLE 2 List of superstructure-related results considering rms values of response indicators (average on eight natural earthquakes)

Structural control strategy	Last-floor disp. $u_{s5}[\mathrm{m}] \cdot 10^{-2}$	First interstory drift $\Delta u_{s2}[\mathrm{m}] \cdot 10^{-4}$	Last-floor total acc. $\ddot{u}_{s5\,tot}\left[\mathrm{m/s^2}\right]$	Base shear V_b [kN]	Kinetic energy T_s [kN m]	Strain energy E_s[kN m]	BIS disp. $u_b[\mathrm{m}] \cdot 10^{-2}$
Conventional BIS (reference solution)	5.91	11.93	0.59	158.30	21.26	0.96	5.46
BIS + TMDI De Domenico and Ricciardi[30]	2.79 −52.8%	6.11 −48.8%	0.35 −40.9%	79.97 −49.5%	8.92 −58.1%	0.35 −63.7%	2.56 −53.2%
Model 2.H Hashimoto et al[34]	3.27 −44.6%	6.14 −48.6%	0.34 −41.9%	80.43 −49.2%	9.42 −55.7%	0.31 −67.1%	3.04 −44.3%
Model 1.H Hashimoto et al[34]	2.94 −50.3%	5.92 −50.4%	0.32 −45.1%	77.96 −50.7%	9.03 −57.6%	0.30 −68.3%	2.71 −50.4%
BIS + nontraditional TMD Xiang and Nishitani[10]	2.93 −50.4%	6.24 −47.7%	0.34 −42.1%	82.14 −48.1%	9.68 −54.5%	0.36 −62.8%	2.69 −50.6%
Model I.S Saitoh[33]	5.06 −14.5%	7.83 −34.4%	0.42 −28.4%	102.12 −35.5%	12.68 −40.4%	0.58 −39.4%	4.76 −12.9%
Model II.S Saitoh[33]	3.52 −40.5%	7.65 −35.9%	0.40 −31.4%	100.80 −36.3%	11.89 −44.1%	0.52 −45.4%	3.22 −40.9%

Note. BIS: base-isolation system; TMD: tuned mass damper; rms: root mean square.

model II.S is the best with regard to the TMD-related response indicators that are listed in Table 3. In addition to the TMD displacement and stroke, in order to qualitatively estimate the production implications and related costs of the different structural control systems, we also listed the reactions of the spring, oil damper, and inertial damper

TABLE 3 List of TMD-related results considering rms values of response indicators (average on eight natural earthquakes)

Structural control strategy	TMD disp. u_t[m] · 10^{-2}	TMD stroke u_{tb}[m] · 10^{-2}	TMD spring reaction R_k [kN]	TMD oil damper reaction R_c [kN]	TMD inertial damper reaction R_b [kN]
BIS + TMDI	4.47	4.52	22.56	13.06	25.32
Model 2.H	4.84	4.60	48.21	18.40	31.33
Model 1.H	5.43	5.21	20.54	13.24	-
BIS + nontraditional TMD	5.39	4.49	23.59	13.13	-
Model I.S	2.44	6.60	73.75	38.00	70.37
Model II.S	3.07	3.87	21.50	4.75	17.51

Note. BIS: base-isolation system; TMD: tuned mass damper; TMDI: tuned mass damper inerter; rms: root mean square.

supporting the TMD, termed R_k, R_c, and R_b, respectively. These reactions are computed with different formulae based on the specific arrangement of the TMD in each model. The very high reactions associated with model I.S are ascribed to the large value of inertance ratio $\beta_t = 0.86$ that is found from the optimization procedure. Also, Saitoh in the original paper[33] considered a $\beta_t = 1.0$ ratio, which is consistent with the aforementioned value. Besides the rms values, we have also computed the max values over the entire time-history duration that, as seen above, are strongly affected by the impulsive character of the accelerograms. Relevant histograms of the last-floor displacement and of the base shear are reported in Figures 14 and 15, respectively. These histograms are organized in a convenient normalized format, by reporting the percentages of reduction as compared to the conventional BIS in the vertical-axis scale. Values lying below the 100% threshold indicate a vibration reduction, whereas the tick marks above each bar specify the actual value for that specific accelerogram. As expected, the max values reductions (of the order of 10–30%) are lower than the rms values reductions due to the time-delay implied in the effective activation of the TMD. The worst reduction performance in terms of last-floor displacement and base shear is achieved for all the six models under the L'Aquila ground motion, due to the high impulsive nature of this accelerogram. In the bar plots of Figure 16, a family of superstructure-related response ratio indicators are reported through average values on the eight considered accelerograms. Superimposed error bars indicate the variability among the eight accelerograms. This variability is reduced due to the adopted scaling of the accelerograms, especially with regard to displacement-related response quantities. Similarly, in Figure 17, a set of TMD-related response quantities are reported (in a nonnormalized format, unlike the previous bar plots).

As stated above, to draw more general conclusions, a larger number of samples is considered. Reference is made to the FEMA P695 far-field record set comprising 44 historically recorded seismic inputs. This set of ground motions has been used to study the seismic behavior of TMD-like systems, see, for example, other studies.[12,46,54] Both the individual response spectra and the median response spectrum (for a 0.05 damping ratio) of this ensemble of inputs are reported in

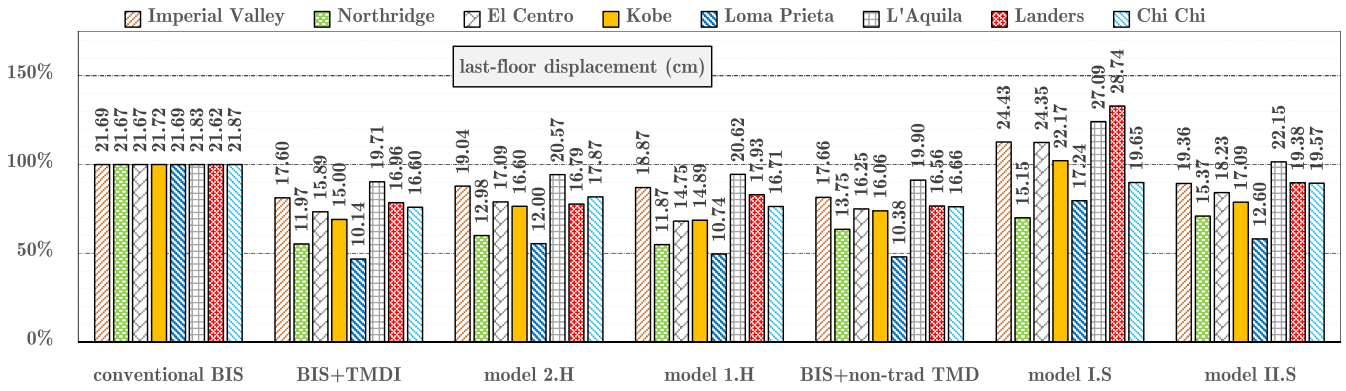

FIGURE 14 Histograms for reduction ratios (compared to conventional BIS) of max last-floor displacement for the six analyzed structural control strategies and for the eight considered accelerograms. BIS: base-isolation system; TMD: tuned mass damper; TMDI: tuned mass damper inerter

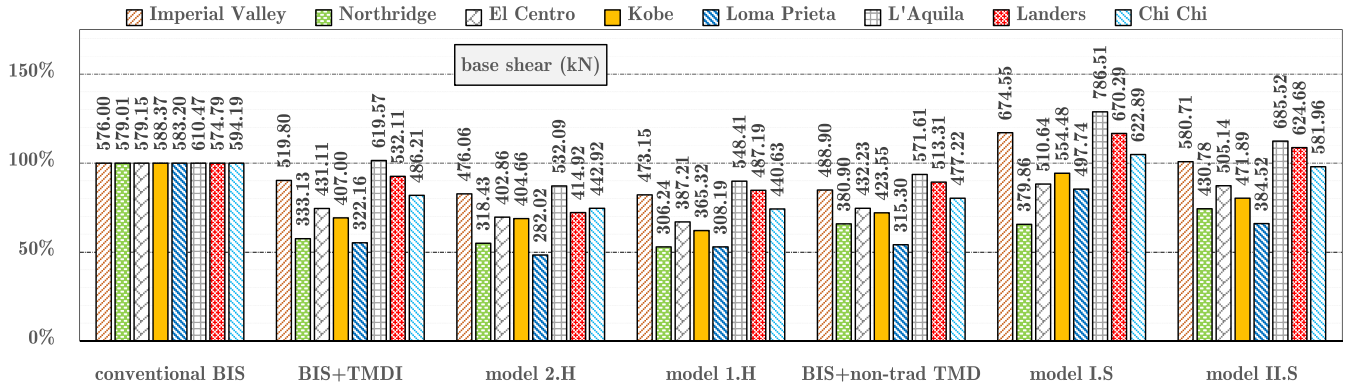

FIGURE 15 Histograms for reduction ratios (compared to conventional BIS) of max base shear for the six analyzed structural control strategies and for the eight considered accelerograms. BIS: base-isolation system; TMD: tuned mass damper; TMDI: tuned mass damper inerter

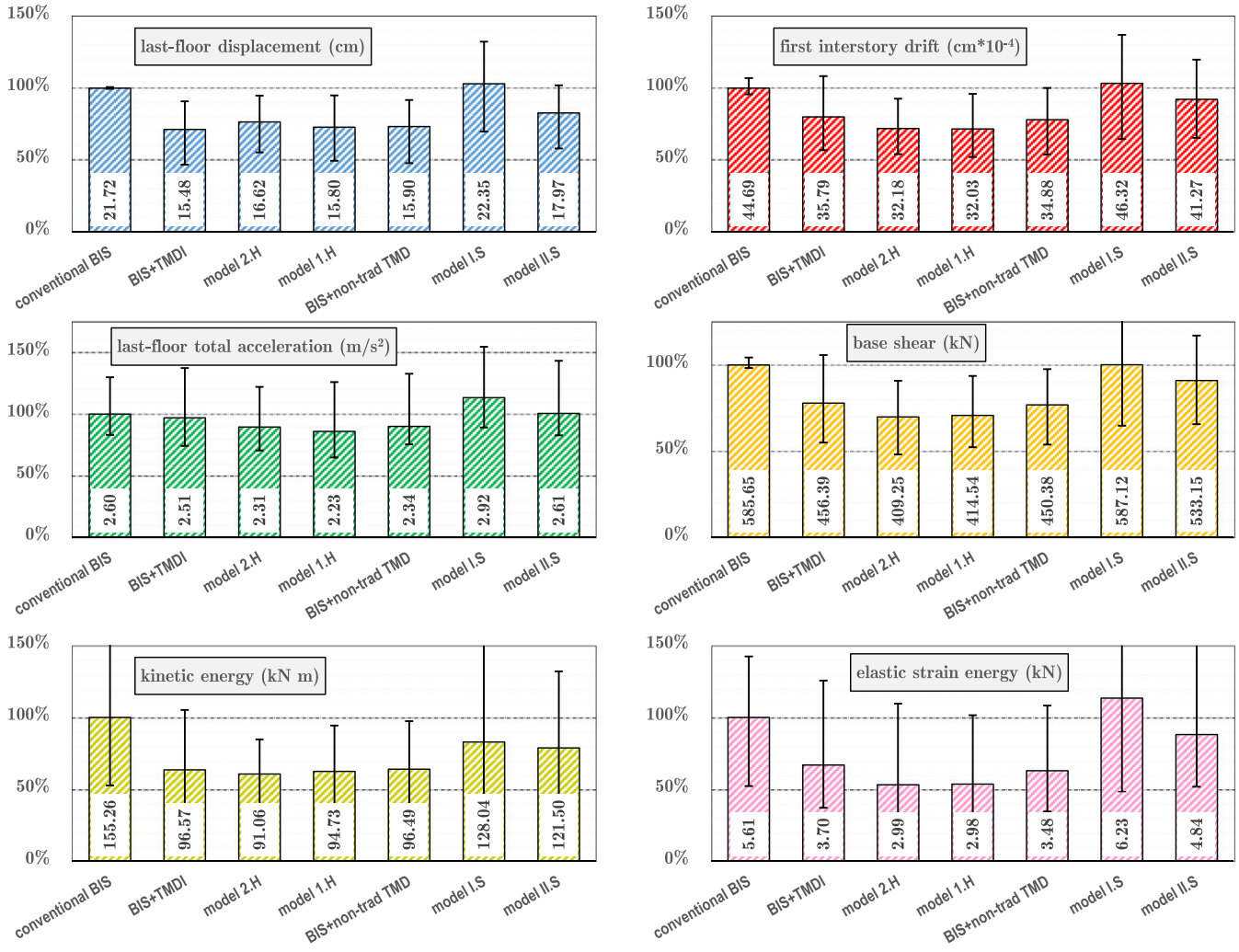

FIGURE 16 Histograms for superstructure-related ratios (compared to conventional BIS) of average max quantities on the eight natural earthquakes. BIS: base-isolation system; TMD: tuned mass damper; TMDI: tuned mass damper inerter

Figure 18. A variety of response indicators have been computed for each ground motion input. Average (over the 44 earthquake ground motions) rms and max values of a few response indicators (relevant to the superstructure, to the BIS, and to the TMD subsystems) are reported in the histograms of Figures 19–21.

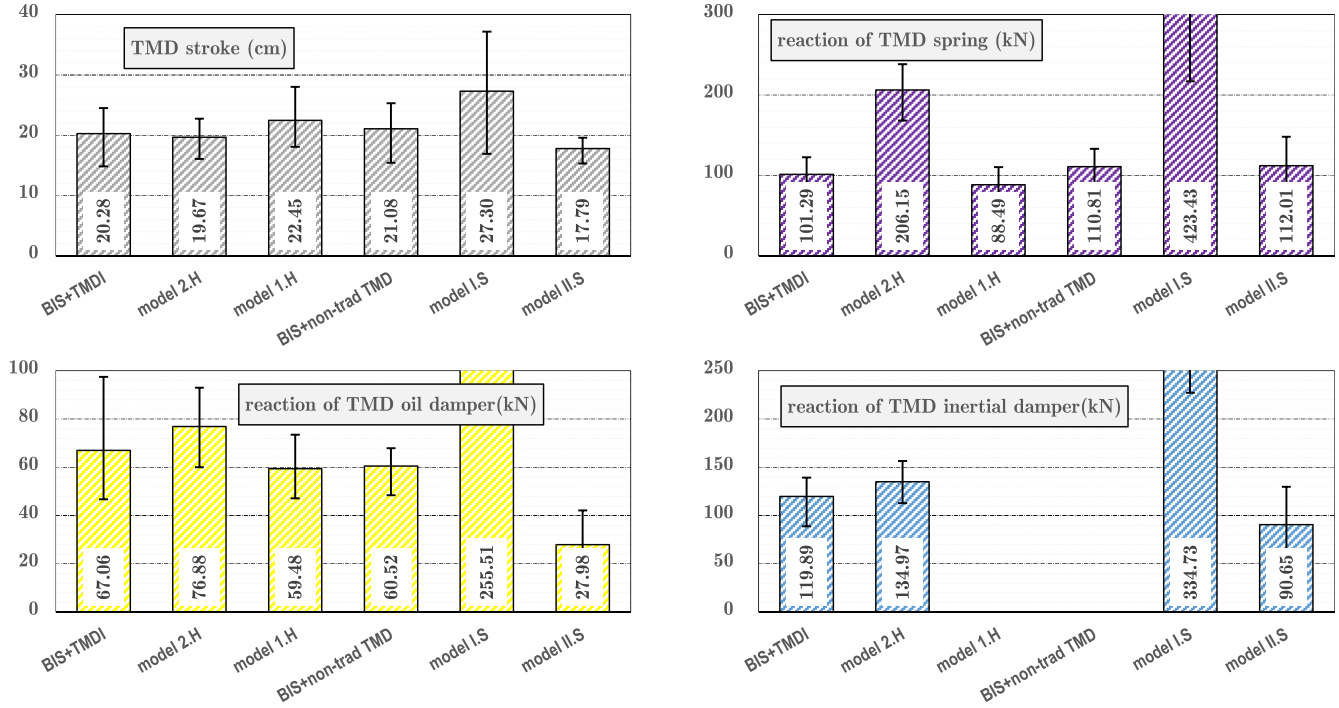

FIGURE 17 Histograms for TMD-related average max response quantities on the eight natural earthquakes. BIS: base-isolation system; TMD: tuned mass damper; TMDI: tuned mass damper inerter

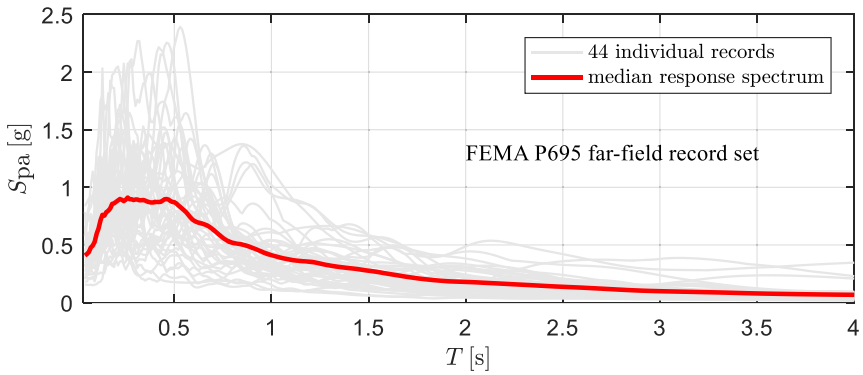

FIGURE 18 Pseudo-acceleration response spectra for the 44 historically recorded ground motions of the FEMA P695 far-field record set[52]

By inspection of the histograms reported in this paper summarizing the results for 52 different seismic inputs, the following general conclusions can be drawn:

- The BIS + TMDI is effective for reducing most of the superstructure-related response indicators and leads to moderate reactions of TMD-related spring, oil damper, and inertial damper.
- Models 2.H and 1.H are the best ones for reductions of superstructure-related indicators (all but last-floor displacement, for which the BIS + TMDI prevails); however, model 2.H yields slightly higher values of reactions in comparison with the BIS + TMDI model, which requires higher costs in terms of TMD-related auxiliary isolators.
- The BIS + nontraditional TMD leads to superstructure- and TMD-related reductions that are in line with those of the BIS + TMDI model. The main difference between these two models is that the involved mass is $\mu_t = 0.2$ instead of $\mu_t = 0.01$, which requires a larger space in the building in order to insert such TMD mass. On the contrary, high inertance ratios can be achieved by simply increasing the gearing ratios of the inerter, which is a key feature that makes the TMDI a lower mass and more effective alternative to the TMD. However, the BIS + nontraditional TMD yields quite similar performance to the BIS + TMD (model 1.H), but with a mass ratio that is halved ($\mu_t = 0.2$ vs. $\mu_t = 0.4$). This is due to the nontraditional (more effective) TMD strategy in comparison with the conventional TMD.[10]

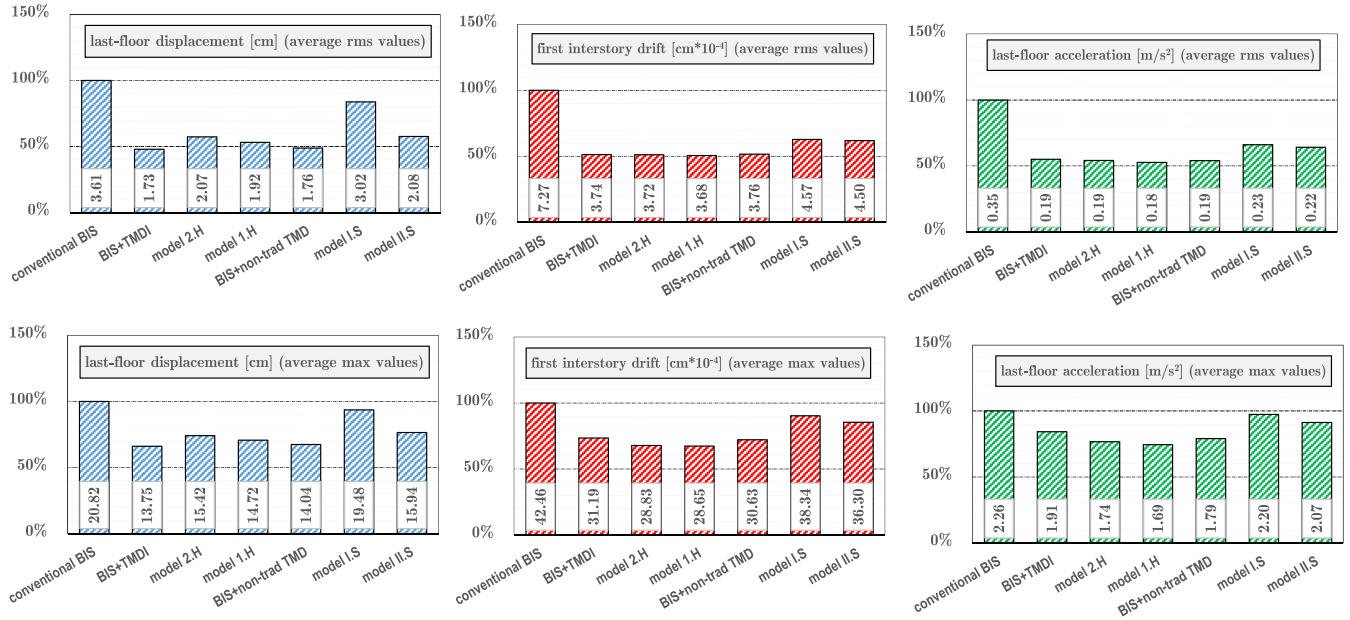

FIGURE 19 Histograms for average rms and max response indicators under the FEMA P695 far-field record set (average values on 44 samples). BIS: base-isolation system; TMD: tuned mass damper; TMDI: tuned mass damper inerter

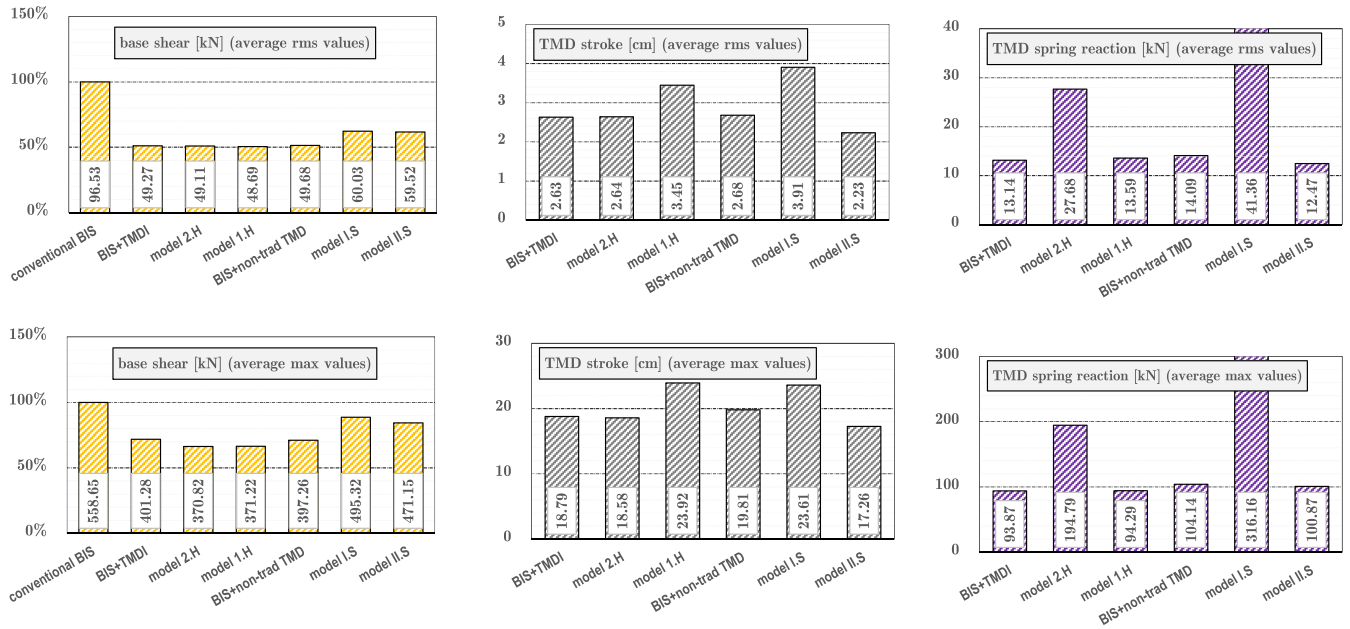

FIGURE 20 Histograms for average rms and max response indicators under the FEMA P695 far-field record set (average values on 44 samples). BIS: base-isolation system; TMD: tuned mass damper; TMDI: tuned mass damper inerter

- Although model I.S is worse than the other models, exhibiting the highest values of reactions, the introduction of the damper in parallel with the inerter in model II.S leads to an improved performance of the system with a significantly lower value of inertance ratio β_t, which is reflected in the significantly lower values of reactions as compared to model I.S. Model II.S is the best one in terms of TMD stroke. Finally, the introduction of the supplemental damper in parallel with the inerter leads to forces that are lower than the oil damper forces reported in the histograms of Figure 17 and Figure 21, which are already the lowest ones among the six models.

On the basis of the results found in this comparative study, the BIS + TMDI and model II.S are the most effective ones in terms of superstructure- and TMD-related response indicators, respectively.

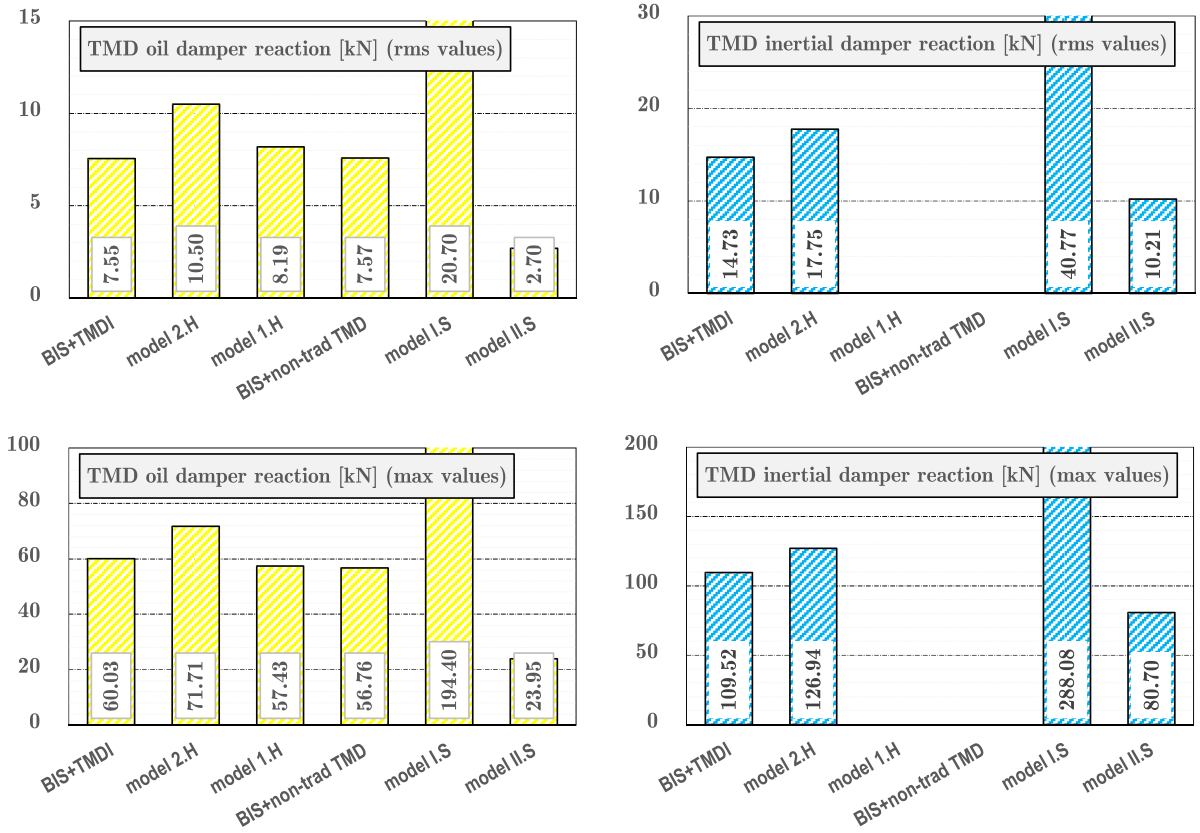

FIGURE 21 Histograms for average rms and max response indicators under the FEMA P695 far-field record set (average values on 44 samples). BIS: base-isolation system; TMD: tuned mass damper; TMDI: tuned mass damper inerter

6 | CONCLUDING REMARKS

A range of structural control strategies that can be implemented to improve the dynamic performance of base-isolated structures have been analyzed and compared. All these strategies imply the presence of a TMD located at basement, below the isolation floor. In addition to the TMD (comprising a spring and a damper element), the presence of inertial dampers has also been investigated in a few schemes to enhance the TMD performance via rotational inertia. Six different models proposed in the literature have been analyzed within a unified framework. Different arrangements of TMD and inerter implemented in base-isolated buildings lead to a totally different dynamic behavior of the structure as a whole.

The FRFs of each model have been derived in closed-form. Guidelines have been provided to select the optimal tuning parameters, by modelling the base acceleration as a stationary Gaussian white-noise random process. The TMD-related optimal parameters for each model have been identified by minimization of the displacement variance but with an eye also for the acceleration variance and for the TMD stroke variance, which is an important response quantity for design purposes and for practical applicability of the damping devices.

Then, the six models have been implemented in a base-isolated multistory building for comparative purposes. The response is computed in the time domain, by direct integration of the equations of motions under a set of 52 historically recorded earthquake ground motions having different spectral characteristics. The seismic performance of the six models has been assessed in terms of a variety of response indicators that are useful and of practical importance for design engineers, including displacements, interstory drifts, floor accelerations, base shear, kinetic, and elastic strain energy, and TMD stroke. In a design process, it is important to foresee the reaction forces associated with the spring, oil damper, and inertial dampers of the TMD. These forces give a preliminary estimate of the costs of each model because higher forces imply larger isolators and/or stiffer elements of connection.

It has been proved that the use of the inerter in conjunction with the TMD according to the TMDI dynamic configuration is a very effective structural control strategy involving a relatively small mass (unlike the classical TMD).

Another effective configuration, especially with regard to the limitation of TMD stroke and TMD-related reactions, is model 2.S in which the auxiliary TMD-related isolators are directly attached to the ground and not placed in between the TMD mass and the BIS, where instead an inerter is placed in parallel to a damper. The nontraditional TMD configuration allows a significant reduction of the TMD mass (in comparison with the traditional TMD—model 1.H) to achieve a target dynamic performance. Finally, model 2.H proves to be the best in terms of reductions of max superstructure-related response indicators, especially total acceleration reductions, despite implying higher values of reactions in comparison with the TMDI model, which in principle requires slightly higher costs in terms of TMD-related auxiliary isolators or devices.

ACKNOWLEDGEMENT

The financial support from the Italian Ministry of Education, University and Research (PRIN Grant 2015TTJN95 and PRIN Grant 2015JW9NJT) is gratefully acknowledged.

ORCID


Dario De Domenico http://orcid.org/0000-0003-1279-9529

REFERENCES

1. Naeim F, Kelly JM. *Design of Seismic Isolated Structures: From Theory to Practice*. New York: John Wiley & Sons; 1999.
2. V. Zayas, S. Low, S. Mahin, The FPS earthquake resisting system. Report No. CB/EERC-87/01, Earthquake Engineering Research Center, University of California, Berkeley, 1987.
3. Anagnostopoulos SA, Spiliopoulos KV. An investigation of earthquake induced pounding between adjacent buildings. *Earthq Eng Struct Dyn*. 1992;21(4):289-302.
4. Heaton TH, Hall JF, Wald DJ, Halling MW. Response of high-rise and base-isolated buildings to a hypothetical Mw 7.0 blind thrust earthquake. *Science*. 1995;267(5195):206-211.
5. Ariga T, Kanno Y, Takewaki I. Resonant behaviour of base-isolated high-rise buildings under long-period ground motions. *Struc Des Tall Spec Build*. 2006;15(3):325-338.
6. Takewaki I, Murakami S, Fujita K, Yoshitomi S, Tsuji M. The 2011 off the Pacific coast of Tohoku earthquake and response of high-rise buildings under long-period ground motions. *Soil Dynamics and Earthquake Engineering*. 2011;31(11):1511-1528.
7. Yang JN, Danielians A, Liu SC. Aseismic hybrid control systems for building structures. *J Eng Mech*. 1991;117(4):836-853.
8. Taniguchi T, Der Kiureghian A, Melkumyan M. Effect of tuned mass damper on displacement demand of base-isolated structures. *Eng Struct*. 2008;30(12):3478-3488.
9. Tsai HC. The effect of tuned-mass dampers on the seismic response of base-isolated structures. *Int J Solids Struct*. 1995;32(8-9):1195-1210.
10. Xiang P, Nishitani A. Optimum design for more effective tuned mass damper system and its application to base-isolated buildings. *Struct Control Health Monit*. 2014;21(1):98-114.
11. Adam C, Di Matteo A, Furtmüller T, Pirrotta A. Earthquake excited base-isolated structures protected by tuned liquid column dampers: design approach and experimental verification. *Procedia Engineering*. 2017;199:1574-1579.
12. Di Matteo A, Furtmüller T, Adam C, Pirrotta A. Optimal design of tuned liquid column dampers for seismic response control of base-isolated structures. *Acta Mechanica*. 2018;229(2):437-454.
13. Casciati F, Giuliano F. Performance of multi-TMD in the towers of suspension bridges. *J Vib Control*. 2009;15(6):821-847.
14. Bortoluzzi D, Casciati S, Elia L, Faravelli L. Design of a TMD solution to mitigate wind-induced local vibrations in an existing timber footbridge. *Smart Struct and Systems*. 2015;16(3):459-478.
15. Giuliano F. Note on the paper "optimum parameters of tuned liquid column–gas damper for mitigation of seismic-induced vibrations of offshore jacket platforms" by Seyed Amin Mousavi, Khosrow Bargi, and Seyed Mehdi Zahrai. *Struct Control Health Monit*. 2013;20(5):852-852.
16. Smith MC. Synthesis of mechanical networks: the inerter. *IEEE Transactions on Automatic Control*. 2002;47(10):1648-1662.
17. Takewaki I, Murakami S, Yoshitomi S, Tsuji M. Fundamental mechanism of earthquake response reduction in building structures with inertial dampers. *Struct Control Health Monit*. 2012;19(6):590-608.
18. Mirza Hessabi R, Mercan O. Investigations of the application of gyro-mass dampers with various types of supplemental dampers for vibration control of building structures. *Eng Struct*. 2016;126:174-186.

19. Ikago K, Saito K, Inoue N. Seismic control of single-degree-of-freedom structure using tuned viscous mass damper. *Earthq Eng Struct Dyn*. 2012;41(3):453-474.
20. Makris N. Basic response functions of simple inertoelastic and inertoviscous models. *J Eng Mech*. 2017;143(11):04017123.
21. Wang M, Sun F. Displacement reduction effect and simplified evaluation method for SDOF systems using a clutching inerter damper. *Earth Eng Struct Dyn*. 2018;2018:1-22. https://doi.org/10.1002/eqe. 3034
22. Makris N, Kampas G. Seismic protection of structures with supplemental rotational inertia. *J of Eng Mech*. 2016;142(11). 04016089
23. Marian L, Giaralis A. Optimal design of a novel tuned mass-damper-inerter (TMDI) passive vibration control configuration for stochastically support-excited structural systems. *Prob Eng Mech*. 2014;38:156-164.
24. Pietrosanti, D, De Angelis, M, Basili, M. Optimal design and performance evaluation of systems with *Tuned Mass Damper Inerter (TMDI), Earthq Eng Struct Dyn*. 2017;46(8): 1367–1388.
25. Giaralis A, Taflanidis AA. Optimal tuned mass-damper-inerter (TMDI) design for seismically excited MDOF structures with model uncertainties based on reliability criteria. *Struct Control Health Monit*. 2018;25(2):e2082.
26. Lazar IF, Neild SA, Wagg DJ. Using an inerter-based device for structural vibration suppression. *Earthq Eng Struct Dyn*. 2014;43(8):1129-1147.
27. Wen Y, Chen Z, Design HX. Evaluation of tuned inerter-based dampers for the seismic control of MDOF structures. *J Struc Eng*. 2016;143(4):04016207.
28. Sun L, Hong D, Chen L. Cables interconnected with tuned inerter damper for vibration mitigation. *Eng Struct*. 2017;151:57-67.
29. Gonzalez-Buelga A, Lazar IF, Jiang JZ, Neild SA, Inman DJ. Assessing the effect of nonlinearities on the performance of a tuned inerter damper. *Struct Control Health Monit*. 2017;24(3):e1879.
30. De Domenico D, Ricciardi G. An enhanced base isolation system equipped with optimal tuned mass damper inerter (TMDI). *Earthq Eng Struct Dyn*. 2018;47(5):1169-1192. https://doi.org/10.1002/eqe. 3011
31. De Domenico D, Impollonia N, Ricciardi G. Soil-dependent optimum design of a new passive vibration control system combining seismic base isolation with tuned inerter damper. *Soil Dynamics and Earthquake Engineering*. 2018;105:37-53.
32. Saito K, Yogo K, Sugimura Y, Nakaminami S, Park K. Application of rotary inertia to displacement reduction for vibration control system. 13th World Conference on Earthquake Engineering 2004; paper #1764, pp. 13.
33. Saitoh M. On the performance of gyro-mass devices for displacement mitigation in base isolation systems. *Struct Control Health Monit*. 2012;19(2):246-259.
34. Hashimoto T, Fujita K, Tsuji M, Takewaki I. Innovative base-isolated building with large mass-ratio TMD at basement for greater earthquake resilience. *Fut Cit Environ*. 2015;1(9):1-19.
35. De Domenico D, Falsone G, Ricciardi G. Improved response-spectrum analysis of base-isolated buildings: a substructure-based response spectrum method. *Eng Struct*. 2018;162:198-212.
36. Chen JB, Liu W, Peng Y, Li J. Stochastic seismic response and reliability analysis of base-isolated structures. *J Earthq Eng*. 2007;11(6):903-924.
37. Masri SF, Caffrey JP. Transient response of a SDOF system with an inerter to nonstationary stochastic excitation. *J Appl Mech*. 2017;84(4):041005.
38. Wang JF, Lin CC, Lian CH. Two-stage optimum design of tuned mass dampers with consideration of stroke. *Struct Control Health Monit*. 2009;16(1):55-72.
39. Krenk S, Høgsberg J. Tuned resonant mass or inerter-based absorbers: unified calibration with quasi-dynamic flexibility and inertia correction. *Proc R Soc a*. 2016;472(2185):20150718.
40. Casciati F, Casciati S, Elia L, Faravelli L. Optimal reduction from an initial sensor deployment along the deck of a cable-stayed bridge. *Smart Structures and Systems*. 2016;17(3):523-539.
41. Casciati S, Faravelli L. Quantity vs. quality in the model order reduction (MOR) of a linear system. *Smart Structures and Systems*. 2014;13(1):99-109.
42. Casciati F, Casciati S. Designing the control law on reduced-order models of large structural systems. *Struct Control Health Monit*. 2016;23(4):707-718.
43. Salvi J, Rizzi E. Optimum tuning of tuned mass dampers for frame structures under earthquake excitation. *Struct Control Health Monit*. 2015;22(4):707-725.
44. Greco R, Marano GC. Optimum design of tuned mass dampers by displacement and energy perspectives. *Soil Dyn Earthq Eng*. 2013;49:243-253.
45. Sadek F, Mohraz B, Taylor AW, Chung RM. A method of estimating the parameters of tuned mass dampers for seismic applications. *Earthq Eng Struct Dyn*. 1997;26(6):617-635.

46. Tributsch A, Adam C. Evaluation and analytical approximation of tuned mass damper performance in an earthquake environment. *Smart Struc Syst*. 2012;10(2):155-179.

47. Schmelzer B, Oberguggenberger M, Adam C. Efficiency of tuned mass dampers with uncertain parameters on the performance of structures under stochastic excitation. *Proc Inst Mech Eng, Part O: J Risk and Reliability*. 2010;224(4):297-308.

48. De Domenico D, Ricciardi G, Benzoni G. Analytical and finite element investigation on the thermo-mechanical coupled response of friction isolators under bidirectional excitation. *Soil Dyn Earthq Eng*. 2018;106:131-147.

49. De Domenico D, Fuschi P, Pardo S, Pisano AA. Strengthening of steel-reinforced concrete structural elements by externally bonded FRP sheets and evaluation of their load carrying capacity. *Compos Struc*. 2014;118:377-384.

50. De Domenico D. RC members strengthened with externally bonded FRP plates: a FE-based limit analysis approach. *Compos Part B Eng*. 2015;71:159-174.

51. Chopra AK. *Dynamics of Structures*. 4th ed. USA: Pearson Prentice Hall; 2012.

52. FEMA P695 (Federal Emergency Management Agency). Quantification of building seismic performance factors. Federal Emergency Management Agency, Washington, D.C.; 2009.

53. Castaldo P, Ripani M. Optimal design of friction pendulum system properties for isolated structures considering different soil conditions. *Soil Dyn Earthq Eng*. 2016;90:74-87.

54. Anajafi H, Medina RA. Comparison of the seismic performance of a partial mass isolation technique with conventional TMD and base-isolation systems under broad-band and narrow-band excitations. *Eng Struct*. 2018;158:110-123.

How to cite this article: De Domenico D, Ricciardi G. Improving the dynamic performance of base-isolated structures via tuned mass damper and inerter devices: A comparative study. *Struct Control Health Monit*. 2018;25:e2234. https://doi.org/10.1002/stc.2234